Directed and on-demand alignment of carbon nanotube : a review toward 3D printing of electronics

Goh, Guo Liang; Agarwala, Shweta; Yeong, Wai Yee

2019

Goh, G. L., Agarwala, S., & Yeong, W. Y. (2019). Directed and on-demand alignment of carbon nanotube : a review toward 3D printing of electronics. Advanced Materials Interfaces, 6(4), 1801318-. doi:10.1002/admi.201801318

https://hdl.handle.net/10356/139762

https://doi.org/10.1002/admi.201801318

DOI: 10.1002/ ((admi.201801318))
Article type: Review

Title: Directed and On-demand Alignment of Carbon Nanotube: A Review Towards 3D Printing of Electronics

*Guo Liang Goh[a], Shweta Agarwala[b], Wai Yee Yeong[c]**

G. L. Goh, Dr. S. Agarwala
[a,b]Singapore Centre for 3D Printing, School of Mechanical and Aerospace Engineering, Nanyang Technological University, 639798, Singapore
Emails: [a] GGOH007@e.ntu.edu.sg, [b] SAGARWALA@ntu.edu.sg

E-mail: [c] wyyeong@ntu.edu.sg
Assoc. Prof. W. Y. Yeong
[c]Singapore Centre for 3D Printing, School of Mechanical and Aerospace Engineering, Nanyang Technological University, 639798, Singapore

Abstract

Carbon nanotubes (CNTs) are one-dimensional nanostructured materials with unique mechanical, optical, and electrical properties which can be potentially exploited for fabricating wide variety of devices. In addition, the biocompatibility of CNTs makes it attractive for wearable and implantable technology applications. Well-aligned CNTs structures show enhanced properties such as superior electron mobility, strain sensitivity, better mechanical property and enhanced performance and reproducibility that are absent in their disordered counterparts, thus allowing more promising applications in various fields. With aligned CNTs, devices can be optimized to exhibit better performance with lesser materials and more miniature designs. This review summarizes the landscape of CNTs alignment, either during the growth or post-growth processing. This paper delineates various CNTs alignment mechanism, process parameters, and challenges of each technique. A comparative discussion on the advantages, disadvantages, and degree of alignment of each technique is presented. A detailed discussion on the various applications that utilize properties of aligned CNTs devices is presented. The advent of 3D printing techniques for printing CNTs for novel and futuristic applications is also discussed.

Keywords: carbon nanotube, nanocomposite, aligned CNTs, 3D printing, additive manufacturing, printed electronics

1. Introduction

Carbon nanotubes (CNTs) are still widely-explored materials today due to their extraordinary intrinsic properties, thus finding applications in wearable electronics, energy storage, and harvesting devices, optoelectronics, chemical sensors, and water filtration. The extreme length-to-diameter ratio, strong covalent bond, and electronic configuration of the one-dimensional (1D) CNT give rise to its superior material characteristics like high electrical and thermal conductivity, mechanical strength, and optical anisotropy. CNTs architectures with a high degree of alignment such as vertically aligned carbon nanotubes (VACNTs) arrays,[1] CNTs sheets,[2] or CNTs ropes[3] provided added advantage

for applications such as chemical sensing and nanoelectronics as they tend to exhibit better performance. For instances, the electron mobility of highly-ordered CNTs film is 43 times higher than random CNTs network and thus the amount of CNTs in nanocomposite can be an order lesser to produce a conducting percolation network when the CNTs are aligned.[4] Also, the strain sensitivity of a well-organized CNTs composite film is 6 times higher compared to the random counterparts.[5] In terms of the mechanical property, the storage modulus of aligned CNTs nanocomposite improved by approximately 40 % as compared to the random CNTs nanocomposite.[6] More importantly, the alignment and uniformity of 1D materials such as CNTs have a significant effect on the performance and reproducibility.[7] Therefore, the ability to obtain aligned CNTs architectures is important for fundamental characterization and potential applications. To date, aligned CNTs can be achieved through various in-situ (in-growth) and ex-situ (post-growth) alignment techniques. The in-situ CNTs alignment technique refers to the class of CNTs where alignment is achieved during the growing process of CNTs, while ex-situ techniques are a class of post-growth alignment process where the CNTs are dispersed in solvent or polymer resin and aligned using external field. Currently, there are more than a dozen CNTs alignment techniques that have been explored and reported. Therefore, understanding the underlying principle of each process is important. This review aims at reporting and analyzing the fundamental mechanisms for various state-of-the-art alignment techniques for CNTs and CNTs devices. Emphasis has been laid on discussing the mechanisms for CNTs alignment through physical and chemical processes , explaining the underlying principle, and showcasing the potential of each technique for different CNTs architectures. Lastly, the state-of-the-art 3D printing of CNTs and the potential of applying CNTs alignment technique to various processes are discussed. In this review, single-walled CNTs (SWNTs), double-walled CNTs (DWNTs), and multi-walled CNTs (MWNTs) will be referred to as CNTs unless otherwise stated.

2. Driving forces for CNTs alignment: theoretical background

The alignment of the CNTs requires a driving torque to change the orientation of the CNTs. The driving torque can be generated by applying external force fields or induced by condition and constraints of the surrounding medium and substance. For instance, the driving torque can be generated by applying shear field, electric field, and magnetic field to the CNTs. Besides, the aligning torque on CNTs can also be induced by van der Waals interaction and a pinned end of CNTs by the tip adsorption to the substrates as shown in **figure 1a** and **1b**. The torque is normally generated to minimize the misalignment angle between 2 adjacent nanotube axes or between the nanotube axis and the force field which is largely attributed to the geometric and electronic structures of the CNTs.[8] The one-dimensional structure of CNTs can be considered as a graphene sheet being rolled into a nano-cylinder. Therefore, CNTs possess similar electronic configuration as graphene sheet that is the hexagonal carbon rings and valence free electrons due to the sp^2 hybridization of the carbon atom. As such, the electrons can flow freely along the wall of the nanotubes and also in the direction of the tube axis.[9] The movement of the electrons circling around the circumference of the nanotubes results in a large orbital magnetic moment and explains the anisotropic susceptibility of CNTs that is responsible for the magnetic-induced torque acting on the CNTs in the presence of magnetic field as shown in **figure 1c**.[10] Thus, they are magnetically symmetric along the tube axis and possess molar susceptibilities parallel ($\chi_{\parallel}$) and perpendicular ($\chi_{\perp}$) to it.[11] For a diamagnetic CNTs with n carbon atoms, the magnetic energy in a magnetic field, the magnetic energy can be expressed as equation (1) with $\chi_{\perp} < \chi_{\parallel} < 0$.[11] As such, the nanotube is most stable when the tube axis is parallel to the magnetic field as the magnetic energy is minimized at H (θ) = 0.

$$E(\theta, H) = -\left(\frac{nH^2}{2}\right)\left[\chi_{\perp} + (\chi_{\parallel} - \chi_{\perp})\cos^2\theta\right] \quad (1)$$

Besides, it is well-known that the van der Waals interaction between CNTs can be explained by the electromagnetic forces between them.[12] The electromagnetic force is formed by the temporary

dipole as a result of the fluctuation of the electron density. It is discovered that the van der Waals potential of CNTs should go as C_3/R^3 with R representing the intermolecular distance.[12] The coefficient C_3 is evaluated at the imaginary frequencies and it is calculated from the dielectric constant of infinite nanotubes and frequency dependent polarizabilities of the molecular fragments.[13] By calculating the minimization of surface free energy of 2 skewed CNTs, the van der Waals torque between them to make them align parallel to each other can be estimated.[14]

Apart from the abovementioned, CNTs in the presence of an electric field can induce dielectrophoretic torque to make them align parallel to the electric field.[15] The polarizability of the elongated CNT is responsible for the formation of dipole across the CNT tube as shown in **figure 1d**.[16] The torque acting on the CNT in an electric field can be estimated by using equation (2).[15]

$$T_{align} = \frac{1}{4}\Omega\varepsilon_m \, Re[\alpha^*]E^2 \, sin\, 2\theta \qquad (2)$$

and,

$$\alpha^* = \frac{\left(\varepsilon_p^* - \varepsilon_m^*\right)^2}{\left[\varepsilon_m^* + \left(\varepsilon_p^* - \varepsilon_m^*\right)L_x\right]\left(\varepsilon_p^* + \varepsilon_m^*\right)}$$

$$\varepsilon_{m,p}^* = \varepsilon_{m,p} - j\frac{\sigma_{m,p}}{\omega}$$

Where Ω is the volume of the particle, ε_m is the permittivity of the surrounding medium, ε_m^* and ε_p^* are complex numbers ($j^2 = -1$) expressed in terms of the electrical permittivities (ε) and conductivities (σ) of the medium (m), and particle (p); E is the magnitude of the electric field; L_x is the depolarization factor, ω is the angular frequency of the electric field ($\omega = 2\pi f$) and 'Re' represents the real part of the complex expression within brackets.

The aforementioned driving forces such as van der Waals' interaction, dielectrophoretic torque, and magnetic-field-induced torque are closely related to the intrinsic property of the CNTs, that is the electron flow within the CNTs. Besides these forces, there are other external forces and torques that can affect CNTs alignment. For instance, the drag force and the Brownian motion of the

particles in a flowing fluid. The former has a strong dependence on the geometric shape of the CNTs and the latter depends on the thermal energy of the medium.[16a]

For CNTs suspended in a medium, the CNTs can experience various forces such as the drag force, the capillary force between the CNTs, and the pulling force by the surface tension of the medium. The drag force of a CNT in a medium depends on its geometry and the viscosity of the medium. In general, the drag force of a rod-like structure such as CNT can be expressed as equation (3).[17]

$$F_{drag=}\, C_D 6\pi\mu R_p U \tag{3}$$

Where C_D is the drag coefficient, μ is the viscosity of the medium, R_p is the CNT radius, U is the particle velocity. The capillary force between the CNTs can be expressed as equation (4).[18]

$$F_{p-p} \sim -\frac{2\pi R_1 R_2 \gamma}{d} \tag{4}$$

Where R_1 and R_2 are particle radii, γ is the surface tension of the medium, and d is the distance between the CNTs. On the other hand, the capillary force ($-\nabla_X E$) and torque ($-\partial E/\partial\phi_p$) due to the surface tension at the interface of fluid can be derived from the capillary energy, $E = -\pi\gamma H_p R_p^2 \frac{1}{R_c(r)} cos\, 2(\varphi_p - \varphi)$ of the elongated body, where H_p is the quadrupole amplitude, R_C is the quadropole distance from the center of the particle, φ_p is the orientation angle of quadrupole and φ is the principle direction of the host interface.[17] This explains why the CNTs tend to be more stable at the solid-fluid interface.[19] This is also the fundamental driving force of the evaporation-driven self-assembly which the mechanism will be discussed in a later section.

For CNTs suspensions that exhibit 2D nematic phase, the governing equation (equation 5) that describes CNTs orientation can be derived from the free energy of the nanotubes, $G = \frac{1}{2}ck_1(\frac{\partial\theta}{\partial x})^2 + \frac{1}{2}ck_2 \sin^2(\theta - \theta_0) + k_bT\, ln\, c$, where the first term is the elastic distortion energy due

to the CNTs interaction and k_1 is the elastic constant; the second term is the surface anchoring energy due to the substrate-CNT interation that prefer a particular tilting angle, θ_0 and k_2 is the phenomenological surface tension constant, the third term is related to the thermal energy of temperature, T, and c is the CNTs concentration. Equation 5 can be expressed as,[20]

$$\frac{\partial^2\theta}{\partial x^2} - \frac{k_2}{2k_1}\mathrm{a}\sin 2(\theta - \theta_0) = 0 \quad (5)$$

A driving torque can also be generated to align the CNTs when the acoustic wave is applied to a CNTs suspension. The aligning moment generated by the nonlinear radiation pressure acting on a straight CNT can be derived as equation 6.[21]

$$M_\theta = \frac{IDL^2}{2}\sin\theta\left(Y_R\sqrt{cos^2\theta + sin^2\Phi sin^2\theta}\right) \quad (6)$$

Where I is the intensity of the acoustic wave, D is the diameter of the CNT, L is the length of the CNT, θ is the azimuth angle on a plane, Φ is the angle from the normal axis of the plane, Y_R is the related to the property of the fluid and the geometry of CNT.

Other aligning mechanisms that exist as a combination of the aforementioned driving forces or require more detailed explanation will be discussed separately in the later sections.

3. Methods for CNTs alignment characterization

Normally, the alignment of the as-grown CNTs films or arrays can be evaluated visually by microscopy technique such as atomic force microscopy (AFM),[22] scanning electron microscopy (SEM),[23] scanning tunneling microscopy (STM)[24], and polarizing microscopy.[25] This technique is especially suitable for samples that have a very thin thickness and low CNTs density which cannot be inspected effectively using other laser-based or x-ray-based technique. Transmission electron microscopy is not suitable because (i) the sample preparation steps could disturb the arrangement of CNTs in the sample and (ii) the small scanning area could not provide the correct information about

the actual alignment of CNTs in the sample. The alignment of CNTs can then be further analyzed by using Fast Fourier transform (FFT) method to evaluate the degree of alignment of the CNTs.[26] Herman orientation factor, f as shown in equation (7) is commonly used to quantify the degree of alignment of the CNTs.[26]

$$f = \frac{3\langle cos^2\delta \rangle - 1}{2} \tag{7}$$

Where $\langle cos^2\delta \rangle$ can be derived from the result of FFT.

The aforementioned techniques are suitable for CNTs that are thoroughly exposed, however not suitable for evaluating the alignment of CNTs embedded inside matrix materials. The alignment of CNTs in composite materials can be evaluated by using Raman spectrometry[27] and XRD spectrometry[28]. For Raman spectrometry, a change in peak amplitude at 1590 cm^{-1} when the orientation of the CNTs sample is adjusted from 0° to 180° indicates there is a preferential alignment of CNTs in the sample. For XRD spectrometry, the alignment of CNTs can be evaluated by plotting the integrated x-ray intensity along the 2θ along the azimuth angle. Generally, 2 peaks can be observed form aligned CNTs and no peaks for the random counterparts. Full-width-half-maximum (FWHM) is normally used to evaluate the degree of alignment of the CNTs, normally, a small FWHM indicates the CNTs sample has a higher degree of alignment. Besides, a more recent study used X-ray CT scan to inspect the 3D texture of CNTs film.[29] Also, a three-dimensional distribution of CNTs network can be inspected by electron tomography with which the orientation of the CNTs can be visualized.[30]

Readers are encouraged to read the textbook and review article by Ren et al.[31] and Iakoubovskii[32] respectively for more information about the techniques for evaluating the alignment of CNTs.

4. Mechanisms of CNTs alignment

4.1 Electrostatic and van der Waals forces-induced CNTs alignment

Chemical vapor deposition technique is commonly used for CNTs fabrication, therefore aligning CNTs in CVD processes are referred to as in-situ alignment technique. Generally, CVD technique can be subcategorized into thermal CVD and plasma-enhanced CVD (PE-CVD) and each of them comes with many variants such as hot-wall CVD, hot-wire CVD, direct-current PE-CVD, radio frequency PE-CVD and microwave PE-CVD, just to name a few.

Vertically aligned CNTs (VA-CNTs) can be grown in CVD process under certain controlled conditions as shown in **figure 2a**. Normally, high growth yield is required for VA-CNTs. This can be achieved by increasing the density of the catalytic nanoparticle deposited on the substrate which is used in the CVD process.[31] Several techniques such as thin film dewetting, solution-based, sublimation, and deposition techniques can be used to prepare closely packed catalytic nanoparticle for the growth substrate.[31] Zhang *et. al.* confirms the effect of catalyst density on the CNTs alignment by showing increasing CNTs spacing results in randomly oriented CNTs.[33] Therefore, it is usually conceived that the van der Waals forces among the densely packed CNTs help in the formation of rigid bundles which support each other from collapsing during the growth.[34] One good advantage of aligning CNTs during growth stage is that CNTs can be grown as long as a few millimeters as the growth front is kept unblocked.[35] The tube length can be controlled by tuning the CVD reaction time.[34] VA-CNTs can be grown from a variety of substrates such as mesoporous silica,[36] channel of aluminum membrane,[37] liquid-crystal matrices,[38] aluminophosphate[39] or zeolites.[40] VA-CNTs stacks can be achieved by repeating water-assisted etching to remove the carbon nanotube cap at its ends and CVD CNTs growth process.[41] Also, the thickness of the catalyst's film plays a significant role in determining the end result of the CVD process. Nessim et al. have shown that thinner catalyst film can lead to the growth of vertically aligned CNTs, whereas thicker film can lead to the growth

of sparse and entangled CNT.[42] Besides, adding a controlled amount of water to the CVD process can result in the growth of VA-SWNTs array with a catalytic selectivity as high as 84%.[43]

Besides, aligned CNTs thin films can be fabricated from CNTs suspension. As CNTs are randomly dispersed in the solution, they are normally functionalized with carboxylic acid group (-COOH) or amine group ($-NH_2$) to provide strong interaction with the substrate to immobilize CNTs on the substrate. Typically, short CNTs with a length shorter than 100 nm is normally used.[44] Like in CVD process, the strong van der Walls interaction between the tail chain of the CNTs molecules forms self-assembled monolayers (SAM) as shown in **figure 2b**. The SAM can be created by using various strategies such as Au-S bonding, surface condensation, and electrostatic interaction. When a nanopattern affinity template is used, CNTs with a length greater than the SWNT-COOH-SAM feature will tend to align along the boundary along the SAM due to electrostatic interaction.[45] Together with direct writing technology, self-aligning printing of CNTs can be achieved by depositing the CNTs-dispersion on-demand onto a SAM-coated substrate for thin film fabrication.[46] An extensive review of VA-CNTs via SAM method can be found in.[44]

4.2 Magnetic field-induced CNT alignment

Magnetic field-induced alignment of CNTs can be achieved in the growth process of CNTs and post-growth process. This method can be considered as remote action as the target substrates can be placed within the vicinity of a magnetic field and do not need to come into contact with any probes. This technique is suitable for the growth of aligned CNTs, alignment of solution-processed CNTs and polymer-CNTs matrix.

For CNTs alignment during the growth process, a magnetic field is used to orientate the catalytic nanoparticle as shown in **figure 3a**.[47] The catalytic nanoparticle is catalytically active on certain nanocrystalline facets and the carbon diffusion rate is highest on those facets. Hence, CNTs can grow preferentially in those directions and alignment can be achieved by manipulating the

orientation of the catalytic nanoparticle. For example, ferromagnetic particles such as iron, nickel, and cobalt have one crystallographic magnetic axis and they tend to align parallel to the magnetic field. Depending on the type of catalytic nanoparticles, CNTs can be aligned in more than one direction concurrently.

Alignment of post-growth CNTs is achievable by placing the solution-processed CNTs in a strong magnetic field as shown in **figure 3b**.[11, 48] Well-dispersed CNTs suspension in a liquid medium is free to rotate and orientate themselves along the field direction when a magnetic field is applied. The CNTs can be dispersed in various liquid media such as DI water, alcohol, dimethylformamide, to form pure CNTs film and liquid polymer to form polymer-CNTs composite materials.[49] The anisotropic magnetic susceptibility of the CNTs produces a magnetic torque which is the driving force for the CNTs alignment. The degree of alignment depends on the competition between the driving force (magnetic torque) and drag forces (hydrodynamic torque and viscous shear).[50] Typically, a magnetic field strength of 10-30 T is required to have properly aligned CNTs.[51] The magnetic sources are normally DC resistive solenoid,[51a] superconducting magnet and MRI magnet bore.[52] Magnetic particles such as iron and nickel can be entrapped in the inner-tubular cavity of CNTs to lower the magnetic field strength required for the alignment to a few Tesla.[53] Unlike the electric field-induced alignment which alters the position of the CNTs, magnetic field-induced alignment orientates the tube only which eliminates CNTs agglomeration.[54] Also, it is suitable for large area alignment of CNTs. Another benefit of using a magnetic field is that it improves the dispersion of CNTs.[55] Furthermore, bundling of CNTs can be promoted by using the magnetic processing technique.[49a]

4.3 Electric field-induced CNT alignment

Similar to magnetic field-induced alignment, the electric field can be applied during both growth and post-growth processes to achieve CNTs alignment. CNTs can be oriented by the electric

field due to their anisotropic polarizability. An electrical torque is generated when an electric field is passed through the CNTs which help orientate the CNTs parallel to the electric field.[15]

In the case of growing aligned CNTs during the growth process, a self-biased electric field can be applied to the substrate to help align the CNTs.[56] An external electric field is normally used to achieve field-directed growth of horizontally aligned CNTs on substrates.[57] Typically, SWCNTs can be field directed along the electric field direction above 130 kV m^{-1} direct-current (DC) field strength or above 250 kV m^{-1} AC field strength. Apart from that, plasma-enhanced CVD (PECVD) is used for the growth of vertically aligned CNTs as shown in **figure 4a**.[58] There is a variety of PECVD, such as radio frequency PECVD,[59] microwave PECVD,[60] hot-filament PECVD,[61] electron cyclotron PECVD,[62] have been developed for this purpose. These methods are used to lower the synthesis temperature of CNTs. In PECVD, the plasma would create a parasitic electric field will help to align the CNTs.

For electric field-induced CNTs alignment of post-growth CNTs, an electrical potential is applied at 2 terminals between the region of interest as shown in **figure 4b**.[23, 63] For bulk CNTs composite, the electric potential is applied to 2 sides of the materials,[64] whereas for CNTs thin film, interdigitated terminals are normally used for unidirectional CNTs alignment.[65] The alignment efficiency depends on the material viscosity, electrical voltage, and electrical frequency.[66] Typically, higher efficiency can be achieved by using a material with low viscosity and applying high electrical voltage and frequency. It has been shown that both DC and AC electric fields work for CNTs alignment.[66-67] However, one disadvantage of using DC electric field for aligning CNTs is that the CNTs in the suspension tend to migrate and accumulate at the terminals causing non-uniform distribution of dried CNTs thin films.[65] Therefore, AC electric field is normally used because it gives better CNTs distribution and requires lower voltage (5.5 kV_{p-p} m^{-1}) comparing to DC electric field (6.6 kV m^{-1}).[66] Besides controlling the peak-to-peak voltage, the AC frequency (typically in the

range of 1-10 MHz) can also be used to control the degree of alignment.[66] Chen et al. found that the CNTs film fabricated in high AC frequency (~MHz) tends to have better degree of alignment and CNTs in low frequency (~hundreds of Hz) tends to form aggregations within the electrode gaps. They also showed that the more tangled CNTs are observed at low AC frequency and the CNTs are straightened out at high AC frequency.[66] Similar result is also obtained by Yamamoto et al..[68] They suggest that the high AC frequency plays a role in suppressing the movements of charged ions in the liquid medium which aids in the formation of a dipole on the CNTs.[68]

4.4 Pulling-induced CNT alignment

Pulling-induced alignment is a method that aligns the CNTs by applying mechanical forces to the CNTs network and the CNTs network can be aligned in the direction of stretching as shown in **figure 5a**.[69] This method is normally used for aligning CNTs embedded in a polymer, however, it can also be used on pure CNTs film.[28, 70] The misaligned CNTs can be realigned by the aligning torque when the force is applied to the ends of the CNTs network. The aligning torque acting on the CNTs can be developed when the force is transferred to the CNTs network in the 2 ways, (i) the stretching of the nanocomposite polymer which results in the formation of shear force at the CNT-polymer interface[71] and (ii) the entanglement at the ends of CNTs within a pure CNTs network.[28] For CNTs embedded in a polymer, the polymer is normally softened first either by melting or dipping in an alcohol solution.[71b] Currently, it has been shown that mechanically straining can effectively align CNTs embedded in different binding materials such as g polyhydroxyaminoether (PHAE),[71b] polyurethane (PU),[72] polypropylene (PP),[73] and polyvinyl alcohol (PVA).[74] Also, the degree of alignment of CNTs improves as the strain increases. Typically, the strain range is typically from 40 % to 80 %. One advantage of this method is that it is very simple. However, this method is time-consuming and highly skill dependent, hence it is unsuitable for industrial applications. Also, it is difficult to ensure homogeneous stretching at the film edges. Besides, pulling method can also be

applied on fiber drawing (spinning) method to fabricate highly aligned CNTs yarns as shown in **figure 5b**. It is found that CNTs aligned better with higher CNTs loading[75] and pulling tension.[76] Besides, Zhang et al. developed a process to treat the CNTs yarn spun from a super-aligned VA-CNTs array with ethanol to make the CNTs more compact and tight.[77] Similarly, Liu et al. spun super-aligned CNTs sheet from a super-aligned VA-CNTs array with tunable tube diameter by controlling the catalyst film thickness.[2] Micro-combing process (by using blades with micro-groove) can be used to mitigate the CNTs waviness, minimizing film defects, and enhancing CNTs alignment and packing.[78] Interestingly, Xiong et al. developed a novel technique that uses a laser source to create strain for CNTs alignment.[79] They attributed the aligning force to the volume shrinkage of the cooling substrate in the laser scanning direction.

4.5 Shear-induced CNTs alignment

Shear-induced alignment can be generated by 3 different kinds of techniques, namely pure shear force alignment, extrusion-induced alignment, and flow-induced alignment. Each technique will be discussed in detail in the following subsections.

4.5.1 Pure shear force CNTs alignment

Shear-induced technique is typically used for post-growth alignment of CNTs. The shear force can be applied in various forms which include cutting, rubbing or pushing as shown in **figure 6**. Shearing induces elastic force which helps align the CNTs.

CNTs alignment by the cutting method is normally used for bulk composite materials.[80] In this method, a knife is used to slice through the target material and CNTs alignment in the cutting direction can be seen on the cut surfaces.[71a] This method is particularly useful for large area production of aligned CNTs thin film and the thickness can be as thin as 50 nm, however, the alignment effect reduces when the film thickness increases beyond 0.5 μm.[80] It is found that this

method is most effective on CNTs with a tube length of several hundred nanometers and diameters <10 nm. However, this method is only applicable to CNTs dispersed resin matrix material of low tube density.

CNTs alignment by rubbing (or pushing) is considered a surface alignment method. This method requires a thin film of vertically aligned CNTs on a substrate either grown from CVD process or prepared from CNTs suspension. The thin film is then rubbed against a plastic surface (Delrin or Teflon) and CNTs alignment can be observed in the rubbing direction.[81] This method is applicable to align CNT with a tube length of 1-5 µm and a diameter of approximately 10 nm. Unlike the cutting method, this method is applicable to pure CNTs thin film and able to produce much densely packed aligned CNTs.[82] Using this method, bucky paper of highly aligned CNTs can be produced.[83] Dry contact transfer technique is another variant of shear-induced technique which also can be used to produce highly aligned CNTs film.[84] Besides, another way of aligning CNTs by shearing method is doctor blade technique which the embedded CNTs in the softened polymer film is scrubbed against a blade or a set of parallel grooves.[82] Miansari et al. deagglomerated dry CNT bundles on a piezoelectric substrate with surface acoustic wave (SAW) and aligned them by shearing against a glass slide.[85] However, one disadvantage of the rubbing technique is that it damages the film. Preparation of post-growth vertically-aligned CNTs can be achieved by peeling off a composite structure with CNTs sandwiched in between 2 polymer membranes.[86] During the peeling process, shear force and mechanical stretch force is applied and acted on the CNTs forcing them to align in the out-of-plane direction. However, the initial orientation of CNTs before the peeling process has a great impact on the alignment effectiveness.

4.5.2 Extrusion-induced CNT alignment

Aligned CNTs fiber can also be produced via the extrusion-based method as shown in **figure 7a**. Normally, the extrusion technique is used to produce long and continuous CNTs yarn or rope.

During extrusion, the CNTs will tend to align themselves in the direction of the drawing, or in other words, in the direction parallel to the orifice. In general, direct spinning, melt fiber spinning and electrospinning can be considered types of extrusion-based technique that can produce aligned CNTs.

Direct spinning of CNTs is a process whereby CNTs are continuously produced in the vapor phase to form a CNTs aerogel, then subsequently spun into CNTs fibers.[76] At the initial stage of the process, the CNTs are synthesized from carbon precursors and catalysts in a reactor. The process consists of various process parameters such as methane flow rate, ferrocene flow rate, sulfur flow rate, hydrogen flow rate, water flow rate, and reaction temperature which requires careful optimization to produce long and mechanically strong CNTs fibers. Direct spinning of CVD can be used to produce aligned nanotube fibers, ribbons, and coating in one step.[65] The full-width-at-half-maximum (FWHM) of the inter-nanotube interference peak was 11°, which indicates the CNTs are highly preferentially aligned in extrusion direction in direct spinning process.[76] The dimension of the extrusion nozzle can be further reduced to 1 μm so that more highly aligned CNTs fiber can be obtained with a higher shear flow.[87] Hossain et al. have shown that ZnO can be used as an alignment agent to promote better CNTs alignment in the CNTs fiber for better mechanical and electrical properties.[88]

Unlike direct spinning, fiber spinning is a multi-step process which could involve preform fabrication or preparation of CNTs dispersion and fiber extrusion. It normally involves the fabrication of CNTs/polymer composite at the first stage and followed by a melt fiber spinning to fabricate the fiber composite. This method can produce highly aligned CNTs fiber with FWHM of as small as 4°. Many polymeric materials can be used for the matrix materials such as poly(methyl methacrylate) (PMMA),[89] polycarbonate,[90] and more.[91] During the process, the matrix material is first melted by heating before fiber drawing. It is found that the fiber drawing speed can be adjusted to vary the CNTs alignment.[75] Another variant of this process is fiber drawing from CNTs dispersion. The

CNTs is extruded into PVA solution from a fine nozzle to form aligned CNTs with PVA coating. A similar method could be used to produce helical fiber structure with a rotating PVA solution bath while the CNTs fiber is being extruded.[91] Liquid crystalline CNTs solution made with dimethyl sulfoxide can be used for the extrusion process to obtain highly aligned CNTs fibers.[92] A similar principle can also be applied to 3D printing and it has been found that the CNTs alignment is affected significantly by the CNTs loading, feed rate, and nozzle diameter.[93]

Electrospinning technique, on the other hand, is a process to produce very fine polymer fiber by extruding the charged polymer resin with strong electric field applied across the extruding nozzle and the target. This method normally produces fine fibers of several hundreds of nanometre. These polymer fibers such as PLA, PAN, PMMA etc. are normally used as carbon precursor for the synthesis of continuous carbon fiber by carbonization process at 1000°C.[94] CNTs can be embedded in the polymer fiber by pre-mixing the CNTs in the polymer resin. The embedded CNTs in the polymer fibers are highly aligned along fiber axis due to the strong electric field in the extrusion process and it is proven effective with both SWNT and MWNT. Typically, the electric field ranges from 0.3 – 200 kV cm^{-1}. The alignment of CNTs in the nanofiber is dependent on the type of polymer used.[95] The electrospun fiber can be made into different forms by using different collectors. For example, electrospun nanofiber in the form of a random non-woven mat can be produced with a flat metal plate as a collector, whereas highly aligned continuous nanofiber can be produced by using a rotating cylinder as a collector.[96]

4.5.3 Flow-induced CNTs alignment

In the thermal CVD process, CNTs growth is affected by the gas flow, be it the feeding gas flow or the convection gas flow.[97] The alignment mechanism is based on 2 major criteria, i.e. the growing front of the nanotube should be free above the substrate surface and the gas flow that directs the CNTs growth direction.[98] The growth direction of CNTs front depends on the competition

between the feeding gas flow and convection gas flow.[99] At low feeding gas flow, the convection gas flow keeps the CNTs growth front away from the substrate surface and make sure that the CNTs is vertically aligned. In contrast, in high feeding gas flow condition, the feeding gas flow dominates, and the CNTs is aligned in the direction of the feeding gas flow. This process is very commonly used to fabricate horizontally aligned CNTs array.[100] Typically for high gas flow condition, stable laminar flow is required to produce aligned long CNTs network as turbulent flow normally produces short and disordered CNTs.[101] The orientation of the substrate in the CVD is not a dominant factor to alter the degree of alignment of the CNTs as the Van der Waals interaction between the SWNTs and silica substrate is stronger than the influence of gravity.[102] Hong et al. also demonstrated the fabrication of horizontally aligned semiconducting SWNTs arrays by illuminating UV radiations to impede the growth of metallic SWNTs during the CVD process.[103]

A thin film of aligned CNT can be fabricated by applying a shear flow to the dispersed CNTs solution as shown in **figure 7b**. This method is applicable to both pure CNTs and polymer/CNTs composite solution. Typically, the CNTs is drop cast on a flat substrate and the shear flow is applied either by gas flow or spin coating method. In the case of gas flow alignment, the CNTs is aligned in the direction of flow direction, whereas for the spin coating method, the CNTs tends to radially with respect to the center of rotation. In both cases, shear flow arises due to the velocity gradient across the thin film. For gas flow alignment, the linear velocity of 6-9 cm/s has been shown to effectively align the CNTs suspension.[104] This method is also found suitable for direct write process such as ink deposition via pipette but alignment can only be done in a large area and limited to a single direction. On the other hand, the alignment of CNTs via spin coating depends greatly on the condition of the substrate surfaces. For instance, better alignment is achieved using amine-functionalized surface than phenyl-functionalized surface.[105] In the case of polymer/CNTs composite, it is found that the CNTs tend to align 45° from the radial direction and independent of radial position and spin rate.[106] The

reported degree of alignment of the CNTs for the rotary spin method is half-maximum-full-width (HMFW) of around <15°.[107] This method is simple and robust; however, it has several limitations such as poor alignment at the center region and no control over the direction of alignment. Besides, it is found that long spin time tends to produce CNTs aggregates especially when the low vapor pressure solvent is used.[108] Aligned CNTs with thin line width can be produced by using the microfluidic method to create a capillary flow of CNTs suspension into the microchannel.[109] Another example of CNTs alignment technique that uses this shearing principle is the blown bubble film technique.[7] Shear flow produced in the dip-coating method can also be used to create CNTs alignment in the direction of the dip direction.[110] This technique creates expanding bubbles by blowing CNTs suspension through a circular mold which results in the aligned CNTs film. The shear stress causes the high aspect ratio CNTs to align in the shearing direction when the CNTs suspension passes through the circumferential edge of the die. Similarly, composite materials of MWNT/polymer can be used in microfluidic infiltration, compression molding, conventional injection molding, micro injection moulding, and microinjection-compression molding processes to create structures with aligned CNTs.[111]

4.6 Self-assembly of Aligned CNTs

4.6.1 Liquid crystal-induced CNTs alignment

Liquid crystal (LC) are soft and ordered structure that can be used to alter the microstructure of materials. Many studies have shown that SWNT and MWNT can be aligned using LC by first creating a well-dispersed CNTs-LC solution. Different classes of LC such as thermotropic LC (display-type) [65, 112] and lyotropic (amphiphilic molecule dispersed in water, e.g. surfactant encapsulated-CNT) LC can be used for CNTs aligning purpose.[113] However, thermotropic LC could not be removed from the CNTs thin film once the alignment is done, whereas the surfactant in lyotropic CNTs-LC can be easily removed by rinsing with water. Generally, LC in nematic phase is

normally used for CNTs alignment purpose.[114] The orientation of the LC can be altered by mechanical, electrical and magnetic forces and hence the CNTs alignment. Depending on how surfactant molecules are attached to the CNTs surfaces, the surfactant-coated CNTs will interact with the host LC solution to promote alignment in a preferential direction with respect to the LC director. CNT concentration is an important criterion for the formation of lyotropic CNTs solution, typically ranges between 1-4 %.[115] One disadvantage of LC-induced CNTs alignment method is that it only works within the certain temperature range of LC's nematic phase. An extensive review of carbon nanotube and liquid crystalline phase has been done by Zakri et al.[116]

4.6.2 CNTs alignment by Evaporation-Driven Self-Assembly

Patterning of CNTs-LC into aligned CNTs thin films is essential to fabricate functional electronic devices. Various techniques have been used to pattern the CNTs-LC such as dip-coating[117] and inkjet printing (**figure 8**),[118] just to name a few. These techniques basically use the principle of evaporation-driven self-assembly of the nanoparticle to control the adsorption of CNTs to the substrate. Generally, there are 2 modes of evaporation, which are (1) constant contact angle (shrinking or depinned contact) and (2) constant contact area (pinned contact).[119] The mode of evaporation is affected by various factors such as rheology of suspension, surface roughness, the rate of evaporation and evaporation mechanism. However, it has been shown that a third mode (switching between mode 1 and 2) is also possible and it is generally believed that it is due to the existence of contact angle hysteresis on the surface.[120] The pinning of the liquid-substrate interface is due to the friction between the substrate surface and the CNTs suspension coupled with the higher evaporation at the interface. The accelerated evaporation rate at the interface causes a capillary flow (also known as convective transport) which brings CNT to the interface forming CNTs aggregates at the liquid edge. This phenomenon is more commonly known as "coffee-ring" effect. Besides pushing the CNTs to the edge, the capillary flow also induces a torque on those CNTs are pinned on one end so that they

align parallel to the interface. This phenomenon can also be attributed to the minimization of the surface energy of the CNTs because the CNTs is more thermodynamically stable along the triple-phase junction line and causing the junction line to be pinned.[121] Due to the equilibrium of van der Waals' force, the CNTs will then stack next to one another.[122] In other words, the first CNT at the interface will act as the LC director to align the subsequent CNTs as the solvent evaporates. Combining the principles of self-assembly and LC-induced alignment, a thin film of highly aligned CNTs can be produced. For the case of inkjet printing, an additional force invoked by the incoming droplets in the printing direction would interfere with the radial capillary force resulting in a total velocity flow which can be resolved in radial direction and printing direction.[122] The effect of the resultant velocity flow is that CNTs would tend to align parallel to it resulting in CNTs being aligned in a preferential direction.[122] The CNTs spacing can be adjusted by varying the concentration of CNTs and surfactant in the suspension.[123] Self-assembly by dip coating is suitable for large area fabrication, however, the process is very slow due to the fact the process depends on the evaporation rate instead of the pulling speed of the substrate.[124] One advantage of evaporation-driven self-assembly method is that non-lyotropic CNTs solution can also be used. This is because local CNTs concentration could exceed the critical concentration when CNTs are pushed toward the periphery via convective transport forming lyotropic CNTs solution locally.[19] Since the alignment is concentration dependent, the CNTs concentration could recede well below the critical concentration in the middle region of the drying CNTs suspension due to the "coffee ring" effect forming randomly oriented CNTs. One way to overcome this issue is to use CNTs suspension with a concentration higher than the critical concentration. Other ways to pattern the CNTs-LC is by using a substrate patterned with different wettability (both hydrophilic and hydrophobic) for CNTs-LC or substrates placing in a wedge configuration.[18, 125] With self-assembled monolayer (SAM) together with inkjet printing, it has been shown that aligned CNTs thin film can be produced using strong wettability

boundary and coffee-stain effect.[126] It was found that CNTs lines with smaller line width can have better CNTs alignment.[125] It is interesting to note that SWNTs tend to align better than MWNTs since SWNTs bend more easily than MWNTs, thus their orientations at the outer edge can be easily adjusted to form a large area well-organized CNTs architectures.[121]

4.6.3 CNTs alignment by Langmuir-Blodgett technique

Langmuir-Blodgett technique is used to create nanostructured thin films on substrates, traditionally used for assembling amphiphilic molecules with a hydrophilic head and hydrophobic tail. This technique involves the transfer of Langmuir monolayer from the liquid-gas interface to a solid substrate that moves vertically through the monolayer (like dip coating). Li et al. used this technique to create highly aligned pristine SWNTs thin films that are suitable for microelectronic devices.[127] The Langmuir monolayer of SWNTs is made by treating the suspension of SWNTs in 1,2-dichloroethane (DCE) solutions with poly(m-phenylenevinylene-co-2,5-dioctoxy-p-phenylenevinylene) (PmPV). The Langmuir monolayer on a water subphase is then repeatedly compressed and retracted to minimize hysteresis. By doing so, the SWNTs will align themselves normal to the direction of the compression and the substrate pulling direction.

4.7 Surface acoustic wave-induced CNTs alignment

Surface acoustic wave (SAW) method can be used to align CNTs suspension horizontally at a preferential angle on a substrate. In this method, the SAW is normally produced by using a piezoelectric transducer or 2 interdigital transducers. Generally, a drop of CNTs dispersion is placed in the cavity between a glass slide and a piezoelectric substrate, $LiNbO_3$. The Rayleigh waves couple into the CNTs dispersion and excites longitudinal pressure wave.[128] This process induces a series of pressure nodes and antinodes with a space of half wavelength, which pushes the CNTs to the pressure node.[129] As such, the spacing of the CNTs can be controlled by adjusting the frequency of the SAW.[130] Due to the piezoelectric effect of the substrate, an electric field is created on the substrate

surface which also helps in aligning the CNTs as shown in **figure 9a**[131] In other words, the direction of the CNTs depends on the resultant field of the acoustic radiation force and electric-field induced force.[129] In some case, the alignment of CNTs suspension on a non-piezoelectric substrate is also possible as shown in **figure 9b**. The degree of CNTs alignment depends on the direction and frequency of the SAW. For instance, better alignment can be achieved with low frequency (several tens of kHz) when SAW travels parallel to the substrate surface.[21] Besides, the substrate-nanotube interaction must be sufficiently weak to avoid rapid adsorption of CNTs on the substrate to achieve good CNTs alignment.[21] Adsorption of CNTs can be improved by applying SAW perpendicularly to the substrate.[21] Interestingly, CNTs can be simultaneously aligned in 2 different directions via SAW method as a result of superpositioning of the SAW from 2 transducers.[132] However, this method is not suitable for CNTs with large curvature.[21]

4.8 Guided growth of CNTs

Besides using electric field and gas flow in a CVD process for in-situ alignment of CNTs, guided growth of CNTs can be done by making use of (i) specific crystallographic plane of crystalline structures or (ii) nano steps on miscut crystallographic planes. This technique commonly involves the use of single crystal silicon (Si),[133] sapphire,[134] and quartz[135] as the substrates for the CVD process. Su et al. found that the CNTs grow in 2 perpendicular directions on Si(100) plane, while the CNTs grow in 3 different directions 60º apart on Si(111) plane.[133] The observation is validated by the molecular simulation using empirical force potentials in which the total interaction energy as a function of nanotubes orientation on the Si plane is investigated.[133] They also found that the CNTs can grow much longer on Si(100) plane as compared to Si(111) plane because the energy barrier for CNTs to slide on Si(100) plane is lower than that of Si(111) plane.[133] Han et al., on the other hand, grew aligned CNTs on a template-free sapphire substrate.[134] They found that the CNTs will preferentially align on a-plane and r-plane of the sapphire substrate, but no alignment is observed on

m-plane and c-plane of the sapphire substrate. Ago et al. attributed the guided growth of CNTs to 2 interactions between the CNTs and the Al atoms in the sapphire which are (i) the electrostatic charge transfer from the Al atom to the C atom and (ii) the formation of covalent bond between the Al and C atoms.[136] Ismach et al. demonstrated the use of a nano-step template to guide the growth of CNTs.[137] The nano-step template is made by miscutting a specific crystallographic plane of a crystal lattice with a slight deviation from the perfect cutting plane.[137] The guided growth of CNTs on the nano-steps can be attributed to the stronger Van der Waal's interaction between the nanotubes and the nano-steps due to larger surface area, the electrostatic interaction between the atomic steps and the induced dipole across the SWNTs; and capillarity of the catalyst nanoparticles at the inner edge of the faceted nano-steps.[138]

In summary, various techniques have been used to achieve aligned CNTs. These techniques include the growth of aligned CNTs via Chemical vapor deposition, and the post-growth alignment via applying a magnetic field and electric field, shearing, straining, fiber drawing/electrospinning, spin coating, liquid crystal, surface acoustic wave, and self-assembly as summarised in Table 1. Table 1 summarizes all the CNTs alignment techniques to the best of authors' knowledge. **Figure 10** shows various in-situ and ex-situ CNTs alignment techniques and their respective resulting end products.

Table 1. Various principle of CNTs alignment and techniques

Principle of alignment (driving force)	Advantages	Disadvantage	During growth/Post-growth	Various processes	Forms of CNTs	Type of alignment	Herman's orientation factor[a] / FWHM[b]	Ref
Electrostatic and Van der Waal's interaction	•Large area coverage •CNTs patterning is possible (by patterning the catalyst or SAM) •Scalable	•Only work with high CNTs density •Not applicable to composite materials	During growth	thermal CVD	Pure CNTs forest	Vertically aligned	0.99	[34]
			Post-growth	Self-assembled monolayers (SAM)	Pure CNTs film	Vertically aligned	0.96	[44]
Magnetic field induced alignment	•Non-contact •Remote action •Applicable to viscous liquids •Improve CNTs dispersion •Prevent agglomeration	•Require very strong magnet (typically >10T) •CNTs must be filled with paramagnetic particles •Unable to control CNT separation	During growth	CVD + magnetic field	Pure CNTs forest	3D aligned	0.61-0.89	[47]
			Post-growth	Pure CNT/CNT composite dispersion + magnetic field	Thin films of SWNTs rope	aligned fiber rope	FWHM (25°-35°)	[51a]
					SWNTs–epoxy composite	3D aligned	0.62-0.95	[52]
Electric field induced alignment	•Fast process (<1minute) •Applicable to viscous liquid	•Electrode/terminal is required •Possible accumulation of CNTs on the electrode •Migration of CNTs can occur •The effectiveness of alignment is dependent on frequency applied	During growth	Plasma-enhanced CVD	Pure MWNTs	Vertically aligned	0.89	[58]
			Post-growth	Pure CNT/CNT composite dispersion + electric field	Pure SWNTs	3D aligned	0.89	[66]
					MWNTs composite	3D aligned	0.94	[64]
Strain-induced alignment	•simple procedure		Post-growth	Stretching Pulling	Pure CNTs film	In-plane	0.83	[28]

	•Controllable degree of alignment by varying strain	•stretching is inhomogeneous at film edge •the sample size is limited •time-consuming •require experience			CNTs composite	In-plane	0.67-0.87	[71b, 72]
					CNT sheets	In-plane	0.99	[2]
					CNT yarns	Aligned yarns	0.99	[77]
Shear-induced alignment (in-plane shear)	•Controllable degree of alignment	•Can incur damage on materials •the degree of alignment depends on the film thickness •only work with low CNTs density	Post-growth	Rubbing	Pure CNT film	In-plane	0.78	[81]
				Domino-pushing	CNTs Bucky paper	In-plane	0.77	[83]
				Doctor blade technique	CNTs/polymer composite	In-plane	0.70	[82]
				Cutting	CNTs composite	In-plane	0.72	[80]
Shear-induced alignment (extrusion-induced)	•fast and simple process •CNTs fiber are highly aligned	•Tend to bend and twist CNTs •Formation of bent and twisted CNTs and agglomerate •Possible fiber formation	During growth	Direct-spinning	Pure SWNTs and MWNTs fiber	aligned fiber rope	0.78	[139]
			Post-growth	Fiber spinning	CNTs/polymer composite	aligned fiber embedded in filament matrix	0.50-0.97	[91]
				Electrospinning	Pure CNTs or CNTs composite	aligned fiber embedded in filament matrix	0.25	[95]
				Nano drawing	Pure CNTs	aligned fiber embedded in filament matrix	0.94	[140]
Shear-induced alignment (flow-induced)	•Simple	•Limited to low viscosity solution	During growth	thermal CVD	Pure CNTs	In-plane and vertically aligned	0.82	[97]

		•the degree of alignment depends on the type of substrates •limited to in-plane alignment	Post-growth	Gas flow	Pure CNTs or CNTs composite	In-Plane	0.87	[141]
				Spin coating	Pure CNTs or CNTs composite	In-Plane	0.54	[108]
				Microfluidic	Pure CNTs	In-Plane	0.53	[109a]
				Blown bubble-film	Pure CNTs	In-Plane	0.85	[7]
Self-assembly and Liquid crystal-induced	•the orientational behavior of carbon nanotubes can be preselected and determined •Can use various techniques such as mechanical, electrical and magnetic forces with a much lower field force •Large area oriented-synthesis of CNT thin film •Densely packed •Suitable for various substrates	•Have a strong tendency towards clustering and aggregation of single tubes into a network •Limited to solution	Post-growth	Dip coating	Pure CNTs	In-plane	0.51	[117]
				Inkjet printing	Pure CNTs	In-plane alignment	0.65-0.91	[123]
				Langmuir-Blodgett technique	Pure CNTs	In-plane alignment	0.84	[127]
Surface acoustic wave-induced	• the spacing of the CNT can be controlled by adjusting the frequency of the SAW	• highly dependent on the substrate-nanotube interaction • not suitable for CNTs with large curvature	Post-growth	Drop-cast	Pure CNTs	In-plane alignment	0.68-0.83	[130], [21]
Guided growth-induced alignment	• In-situ alignment	• Low CNT density	During growth	• Lattice-guided • Nano-steps guided	Pure CNTs	In-plane	Most CNTs fall within ±5° Angle deviation from the aligning angle	[136]

[a)]Herman Orientation Factor: the value of 1 represents perfect alignment; the value of 0 represents random alignment. This Herman Orientation Factor is obtained by extracting the SEM images from the original article and then processed by using the image processing software, ImageJ.
[b)]Full With Half Maximum: smaller angle deviation suggests better alignment.

5. Properties and Applications of aligned CNTs

5.1 Composite materials and structures

Composite material refers to an engineered material that is made up of a combination of 2 or more different constituent materials, normally fiber and matrix. Generally, the fiber normally has a high tensile strength to withstand the mechanical load, whereas the matrix transfers the load to the fiber and maintain and hold the fiber in place at the same time. Composite has become popular in many fields such as building, aerospace, and automobile because it is cheaper, stronger and lighter. CNTs/polymer composite, being the most suitable candidate for composite materials, have been widely studied because of its enhanced mechanical property, heat transfer and electrical property.[142] These CNTs/polymer composite can be made into different forms such as composite fibers, fabrics, sheets, films, filaments, and structure. CNTs/polymer composite with the CNTs aligned in a specific direction can further enhance the mechanical, thermal and electrical properties along the CNTs axial direction.[143] This allows the flexibility to design the property of the structure by controlling the CNTs orientation which cannot be achieved by conventional materials. Some application of composite materials with aligned CNTs are sports equipment, electrostatic dissipation (ESD) and electromagnetic interference (EMI) shielding.[144]

5.1.1 Enhanced mechanical property

Miaudet et al. reported composite nanotube fibers with very large strain-to-failure (430 %) and high toughness (870 J g^{-1}).[145] To improve the CNTs alignment in the fibers, they developed a hot drawing method to fabricate highly aligned composite fiber. Using this technique, the CNTs alignment of hot drawn CNTs/PVA fibers is shown to improve from ±27° to ±4.3°. This makes the aligned CNTs/PVA fibers less sensitive to moisture and capable of maintaining high toughness in humid condition.

Khan et al. have fabricated epoxy nanocomposite with aligned CNTs using DC electric field.[67] They have shown that Young's modulus and fracture toughness of the epoxy nanocomposite with aligned were shown to be 22 % and 30 % respectively higher (along the nanotube axis) than those with randomly oriented CNT (**figure 11a &11b**). Also, they have noted the threshold concentration of the CNTs concentration to be 0.3 w%, beyond which the material property of the epoxy nanocomposite deteriorates. Besides, the Storage modulus of the epoxy nanocomposites also show a similar trend as Young's modulus (**figure 11c**), however, they noted that storage modulus in the transverse direction of the epoxy nanocomposite is lower than randomly-oriented nanocomposite. This can be explained by the lower constraint in polymer chain motion in the direction perpendicular to the aligned CNTs.

He et al. have fabricated epoxy nanocomposite with aligned CNTs with a 0.7 T magnet.[49e] They have shown that the crack density in the nanocomposite is significantly reduced by 37.2 % and the suppression to microcracks also is increased by aligning the CNTs perpendicularly to the crack propagation. Besides, aligned CNTs can also be used to enhance the interlaminar property of laminates structure by about 9 %.[146]

Wang et al. reported a methodology to improve the strength and stiffness of aligned CNTs/Nylon composite by drawing and stretching approach.[147] The ultimate strength of the CNTs/Nylon composite improved by 50%, 150%, and 190% corresponding to stretch ratio of 2%, 4%, and 7%, respectively. The improvement in the mechanical property can be explained by the reduction of waviness in the CNTs and hence the improvement in the alignment of CNTs.

5.1.2 Enhanced heat transfer

Choi et al. fabricated an aligned CNTs-PMMA composite with 3 w% of SWNTs dispersed in uncured epoxy resin using magnetic field as driving force.[49a] They observed a 300 % increase in thermal conductivity with the addition of 3 w% of SWNT as compared to the pure PMMA and a

30 % increase in thermal conductivity (4 W m^{-1} K^{-1}) in the direction of the magnetic field (25T) as compared to the nonaligned CNTs-PMMA samples. However, it has been suggested by the authors that the bundling effect (which is promoted by the magnetic field) would work against the enhancement of thermal conductivity of the composite materials.

Gonnet et al. developed a fabrication technique for nanotube/polymer composite which is by embedding magnetically aligned buckypaper into a low viscosity polymer resin (**figure 11d**).[148] They have shown that for the pristine aligned buckypaper mats, the thermal conductivity is relatively high (42 W m^{-1} K^{-1} at room temperature), with an anisotropy $K^{\parallel}/K^{\perp}$ ~ 3.5. Also, their result also shows that the thermal conductivity of the aligned nanotube composite is 50-100 % higher than the random nanotube composite.

Marconnet et al. investigated the thermal conduction in aligned CNTs/polymer composite with high packing density made by biaxial mechanical compression method.[149] They found out that the thermal conduction of the nanocomposite enhances by a factor of 18 by adding 17 vol% of CNTs to the base epoxy. Similarly, the observed an anisotropy in the thermal conduction of $K^{\parallel}/K^{\perp}$ ~ 2-5 with greater anisotropy at higher CNTs volume fractions.

Huang et al. studied the thermal conductivities of the aligned and dispersed CNTs/silicone composite.[150] They have found that the thermal conductivities of pure silicone matrix (0.56 W m^{-1} K^{-1}) and dispersed CNTs/silicone composite (0.59 W m^{-1} K^{-1}) are rather similar, however the aligned CNT/silicone composite (1.21 W m^{-1} K^{-1}) exhibit about 115 % enhancement in thermal conductivity.

Park et al. showed that the thermal conductivity of the long MWNTs/epoxy composite is 55 W/mK higher compared to the short-MWNTs counterpart.[151] Also, they have demonstrated that the degree of alignment of CNT can be improved by mechanical stretching which then enhances the thermal conductivity to over 100 W/mK.

5.1.3 Enhanced electrical conductivity

Li et al. produced woven CNTs fabric from CNTs using direct spinning and achieved best electrical conductivity they have measured along a fiber was $8.3 \times 10^5\ \Omega^{-1}\ m^{-1}$, which is better than conventional carbon fiber.[76]

Khan et al. fabricated epoxy composite with aligned CNTs and showed that the electrical conductivity of epoxy nanocomposite with aligned CNT exhibits at least 1 order magnitude higher than that or randomly oriented nanocomposite (**figure 11e**).[67] They also found out that the percolation threshold for epoxy nanocomposite threshold in the transverse direction (perpendicular to CNTs alignment direction) is about 0.05 w% which is approximately an order higher than that in the parallel direction. The electrical conductivity of 0.5 w% epoxy nanocomposite is the reported to be around 10^{-3} S cm^{-1}. The anisotropy in percolation results in the difference in the electrical conductivity in both parallel and transverse direction of the epoxy nanocomposite. Interestingly, the anisotropy in electrical conductivity diminishes as the CNTs increases due to the increasing interconnection in the transverse direction.

Shang et al. have developed a highly stretchable CNTs/polyurethane conductive nanocomposites can that be stretched up to approximately 550 % before breaking.[72] They have demonstrated that the CNT in the composite can be realigned by applying mechanical stretching force to the specimen. The conductive nanocomposites have an electrical conductivity of around 5 S cm^{-1} and able to retain its electrical conductivity after being stretched repeatedly at 20 %.

5.2 Electrical and electronic devices

5.2.1 Electrodes for energy storage device and energy harvesting device

Battery and supercapacitor, known for their high energy density and power density, are the common energy storage devices that are often used to power electronic devices. However, conventional electrodes for these energy storage devices have certain limitations that restrict the device performance. For instance, battery with an active binder in the electrodes normally suffers

from non-uniform porosity, inhomogeneity, tortuous electrolyte diffusion paths, and high electrical and thermal resistance caused by the point contacts between individual particles.[152] Thus, the attribute of the high specific surface area and electrical conductivity of CNTs makes them good candidates for battery and supercapacitor electrodes.[153] Commonly, CNTs is used as electrodes for lithium-ion battery,[152, 154] lithium-sulfur battery,[155] pseudocapacitors,[156] and electrical double layer capacitor.[153-154] As electrodes of energy storage device, aligned CNTs electrodes are much preferred over entangled CNTs electrodes because of their higher specific capacitance, lower equivalent series resistance, and better rate capability than the entangled CNTs electrodes. This is because aligned CNTs electrodes possess larger pore size, more regular pore structure and conducting pathway.[157] The VA-CNTs electrode can be directly grown on Inconel disk[158] or metal foil [155a] and, in certain cases, can be further processed into free-standing thin film,[159] fiber,[160] and yarn[161] (**figure 12A**) for wearable and stretchable devices [153]. For pure CNT electrodes, the performance of the supercapacitor can be improved by the densification process using liquid drops.[162] The densification process reduces the lateral volume significantly while retaining the original surface area of CNTs which considerably increases the volumetric adsorption density. One limitation of CNTs is the poor wetting behavior at the electrode/electrolyte interface. The wetting behavior can be improved by plasma and force vacuum wetting procedures.[153] To further improve the performance of the energy storage device, composites electrodes such as CNTs/transition metal (molybdenum disulfide),[163] CNTs/metal oxide (Fe_3O_4, MnO_2, oxidized nickel),[156, 159, 164] CNTs/semi-conducting metal (silicon),[165] CNTs/non-metal (sulfur),[155c] and CNTs/ polymer (Polyaniline, PEDOT/PVDF)[166] have been explored to enhance the capacity and power delivery. However, these metal oxide composites often face issues such as the poor conductivity of oxides that lowers the rate performance, and degradation of the cell's capacity due to the change in volume and aggregation of the oxides. Therefore, cross stack CNTs film is normally used for these electrodes loaded with metal

oxide nanoparticles.[142] The fabricated Li-S battery with silicon/carbon-coated VA-CNTs can carry over 3000 mA h g^{-1} with virtually no sign of degradation after over 250 cycles.[152] Recently, nickel cobaltite has become a popular candidate for supercapacitor to be integrated with VA-CNTs and showed a specific capacitance of 970 Fg^{-1} at 2 Ag^{-1} with capacity retention of over 80 % for more than 3000 cycles.[153] Izadi-Najafabadi et al. reported a binder-free SWNTs supercapacitor that can operate at a higher voltage (4 V) which can deliver higher energy and power performance with a specific capacitance of 160 Fg^{-1}.[167] Besides, they also found that the aligned SWNTs array performs best when oriented parallel to the dominant ion transport direction.[168]

Interestingly, CNTs can be used to produce the high-efficiency silicon Schottky solar cells. Aligned CNTs has been proven to increase the CNTs-Si junction density and allows faster transport paths for photocurrent in the oxide.[169] It has been shown that the aligned CNTs can achieve an efficiency of up to 10.5 %, which is higher than the counterpart with randomly oriented CNTs network.[170]

5.2.2 Field-emission devices

CNTs can be used for field-emission devices due to its high aspect ratio and small tip radius of curvature.[171] The unique structure of CNTs has resulted in high field enhancement ranging from 1000 to 3000.[172] The field emission property of VA-CNTs is influenced by CNTs length and spacing. For a given length of CNTs, the macroscopic electric field is reduced when the spacing of CNTs is increased. On the other hand, for a certain spacing of CNTs, the macroscopic electric field is reduced when the length of CNTs is increased. However, it is not true for very high-density CNTs film.[172] Besides, the orientation of the CNTs orientation to the substrates also have a significant effect on the field emission, for instance, the VA-CNTs can exhibit much better field emission as compared to horizontally aligned CNTs.[173]

Song et al. fabricated a well-aligned CNTs array and investigated its field emission property.[174] The vertically aligned CNTs array is fabricated by the CVD process and the field emitting area is measured to be 4.0×10^{-5} cm^2. They have the best-reported result with a large current density as high as 80 mA cm^{-2} at 3V μm^{-1}. Jung et al. developed a flexible field-emission device with aligned CNTs using silicone rubber as base materials (**figure 12B**).[175] They have demonstrated that their field-emission device exhibits a field-enhancement factor of approximately 19100 with a turn-on field of 0.87 V μm^{-1} and a current density of 1 mA cm^{-2} at 0.76 V μm^{-1}. The composite materials remain electrically functional even after being strained up to 12 % repeatedly.

Generally, CNTs-based field emission displays (FEDs) often face challenges as follow: (1) SWNTs have low voltage threshold but short emission lifetime and (2) MWNTs have good emission lifetime but high voltage threshold.[176] Double-walled carbon nanotubes (DWNTs) emitter possess the good quality of both SWNTs and MWNTs, that is low voltage threshold and long emission lifetime.[177] Tamada et al. reported a water-assisted CVD process to fabricate VA-CNTs arrays of DWNTs from iron catalysts.[178] The VA-DWNTs forest is measured to be 2.2 mm high and the percentage of DWNTs is found to be as high as 85 % with an optimum film thickness of iron catalysts.

5.2.3 Field-effect transistor

Semiconducting CNTs is suitable for field-effect transistor because of its high mobility.[179] The key challenges in faced in fabricating CNTs-FET is the difficulty in placing and aligning the CNTs over a large area and low on/off ratio due to the mixing of metallic CNTs. Due to the high resistance of the CNTs (~1.4 MΩ sq^{-1}), the CNT-FET often exhibit undesirable low-level on-state drive current.[124] Very often, metallic CNTs is added to the CNTs-FET to improve the on-state drive current at the expense of lowering the on/off ratio (1 – 2 order of magnitude). As such, controlling the CNTs alignment in the CNTs-FET is very important.

Engel et al. developed a large area fabrication technique for CNTs-based thin film transistor using self-assembly technique (**figure 12C**).[124] The technique takes advantage of the liquid crystal nature of the CNTs dispersion to fabricate a thin film of aligned semiconducting CNTs with directionality error within 5°. Besides, the highly dense and aligned CNTs transistor has on-state performance is very good, delivering high drive currents, I_{on}=1 mA at V_{sd}=2 V, while maintaining I_{on}/I_{off} ~ 10^3. Li et al. used AC electrophoresis method to the deposited SWNT to selectively remove the metallic SWNT by current induced oxidation.[105] By applying the AC voltage to the CNTs-FET, the orientation, length, and reconnection of the CNTs can be controlled. The back-gate CNTs-FET has an on/off ratio of 7 x10^5 at Vds =150 mV. LeMieux et al. showed that the CNTs in the CNTs-FET can be aligned using spin-coating method.[180] The density and the alignment of the CNTs can be tuned by using different functionalized surfaces. The fabricated CNTs-FET exhibits a high on/off ratio of 9 x10^5.

Kang et al. reported a transistor made up of ~2100 SWNTs on interdigitated electrodes with a measured transconductance of the device approaches 1,000 cm^2 V^{-1} s^{-1} and 3,000 S m^{-1}, respectively, and with current outputs of up to 1 A.[181] Transistor with aligned CNT arrays is also found to be suitable for radio frequency (RF) devices. Kocabas et al. reported a transistor with sub-micrometer channel length exhibits unity current gain and unity power gain frequencies as ~5 GHz and ~9 GHz respectively.[182]

5.2.4 Optoelectronics

Aligned CNTs films have been widely used in optoelectronics due to its unique such as its high transparency, light polarizability, and electrical conductivity. For instance, aligned CNTs films have been reported to be used as polarizer, polarized light source, alignment layer for liquid crystal display and transparent electrodes.

Due to the unidirectional feature of the aligned CNTs, some polarizing effect can be observed in electromagnetic wave absorption and emission behaviors.[183] The polarizing effect of aligned

CNTs film can be explained by the photon absorption characteristic at different incident angles.[184] The electrons can flow in the same direction as the E-field of a photon if the polarization of the incident photon is parallel to the tube axis. As a result, the photon energy will then be absorbed by the electrons and dissipated as heat energy. On the other hand, the energy of an incident photon with polarization transverses the tube axis cannot be absorbed by the electrons and hence the polarizing effect.[142] Typically, the CNTs-based polarizers are fabricated by drawing from VA-CNTs array. It has been shown that the transmittance of the CNTs-based polarizer is affected by the height of the VA-CNTs array, whereas the degree of polarization is affected by the drawing angle during the film formation process.[185] The degree of polarization (0 represents no polarization, 1 represents perfectly polarized) can also be improved (0.5 for 1 layer; 0.99 for 3 layers) by stacking multiple aligned CNTs film in the same orientation.[186] Ren et al. reported a CNTs-based terahertz linear polarizer with a degree of polarization in terms of absorbance were 1 and the reduced linear dichroism was 3, throughout the entire frequency range of 0.1-1.8 THz.[187] By applying DC electric current to the aligned CNTs film, it can emit polarized visible light. The degree of polarization of the emitted light is affected by the drawing angle, i.e. higher the degree of polarization at larger drawing angle.[185, 188] Besides, the degree of polarization can be tuned by stretching the CNTs/PVA composite film polarizer.[189]

The alignment layer of liquid crystal display (LCD) is vital to control the liquid crystal (LC) orientation. Conventionally, the alignment layer is fabricated by mechanical rubbing of the surface of polyimide films. Parallel grooves formed during the rubbing process can be used to direct the LC orientation. By the same token, nano grooves formed between the unidirectional nanostructure of the aligned CNTs film can be used to direct the LC orientation.[190] Several ways have been proposed to create the aligned CNTs film for alignment layers, which are drawing method,[190] self-assembly and dip coating method.[110] For the drawing method, the aligned CNTs film is first wetted by a volatile

solvent and placed on a substrate. After being dried in ambient condition, the CNTs films attach firmly to the substrate by van der Waal's interaction and coating of silicon dioxide can be done to further prevent delamination.[190] Aqueous dispersions of CNTs are used for both self-assembly and dip coating methods. However, both techniques create very distinct film morphology with self-assembly (gradual evaporation) produces a densely packed CNTs film and dip coating (constant dip rate) produces sparse CNTs film. Due to the high transparency and electrical conductivity of the CNTs film, the CNTs alignment layer can be used directly for LCD. Russell et al. have developed a technique that used aligned CNTs film as a template and sacrificial layer for silicon nitride target layer. The CNTs film is then removed by thermal treatment to create silicon nitride alignment layer with improved transmittance. Aside from acting as a transparent alignment layer, the resistive nature of the CNTs film can be made used to act as a built-in heater to widen the operating temperature of the LCD.[190] Kang et al. developed a transfer printing method to fabricate multilayer superstructures of a large collection of SWNTs arrays configured in aligned and random CNT networks on various substrates suitable for optoelectronic devices.[191]

In short, CNTs can be used and incorporated directly into LCD panel. Liu et al. found that CNTs film in the vacuum can be heated to glow and cooled down by applying and cut off the voltage with fast switching time (~1ms).[192] With proper sealing, they have fabricated a 16 x 16 pixels CNTs film incandescence display with each pixel giving a brightness of 6400 cd m^{-2} at 0.08 W (**figure 12D**). Besides, the LCD can be doped with a small amount of CNTs (CNTs are aligned along the nematic LC director) to modify the twist elastic constant and rotational viscosity and hence improving the response time of the LCD.[193] Aside from displays, the aligned CNTs/PET composite film produced by roll-to-roll technique can also be used as the top and bottom transparent conducting layers of a touch panel (**figure 12F**).[194] Needless to say, aligned CNTs is important in the field of optoelectronics and have found many useful applications.

Besides being able to be used as optoelectronics, VA-CNTs arrays can be used as a black body absorber. The VA-CNTs array is found to be able to absorb light almost perfectly across a very wide spectral range (0.2-200 μm). This can be attributed to the VA-CNTs array structure which is the sparseness and imperfect alignment of the VA-CNTs.[195]

5.2.5 Electromechanical devices

Electromechanical devices refer to devices that can convert an electrical signal into mechanical motion or vice versa. Carbon nanotubes have been found suitable to be used as transparent and flexible electromechanical devices. Some applications of CNTs-based electromechanical devices are strain sensor, microphone, loudspeaker, and actuator.[196]

Xiao et al. developed a flexible, stretchable and transparent carbon nanotube thin film loudspeaker based on the thermoacoustic effect (**figure 12E**).[196c] The highly aligned CNTs thin film (fabricated simply by drawing method) can generate loud sound once being fed by electrically current with frequencies within the audible range. It has been shown that the CNTs-based loudspeaker has wide frequency response (100 - 100 kHz) and very high sound pressure level (up to 100 dB with an input power of 4.5 W) due to the ultra-small heat capacity of the CNTs thin film ($6.4\text{-}8.9 \times 10^{-3}$ J m^{-2} K^{-1}). The fabricated aligned CNTs thin film possesses many other advantages such as optically transparent, stretchable, and magnet free. Besides, the nanometer-thick CNTs thin film is free standing and can be easily made into different shape and sizes to cater for many other acoustic applications.

Aliev et al. developed an actuator that is capable of producing large stroke using a CNTs-aerogel sheet (**figure 12E**).[196e] The CNTs-aerogel sheet can be used as an electrically powered artificial muscle that is controlled by voltage and is able to provide a large elongation of 220 % and fast elongation rate (3.7×10^4 % per second). The density of the CNTs-aerogel sheet is reported to be as low as 1.5 mg cm^{-3} and the specific strength in the direction parallel to the CNTs is higher than

that of steel. Comparing to conventional rubber, the CNTs-based actuator has a Poison's ratio of 15 which is 30 times higher than the counterpart. The large Poison's ratio of the aligned CNTs film gives rise to its unique property like the negative linear compressibility and the ability to be densified when stretched.

Foroughi et al. fabricated a torsional carbon nanotube artificial muscle with twisted CNTs yarns.[197] The CNTs-based torsional actuator is filled with electrolyte and operates like a simple 3 electrodes electrochemical system. The thinner-than-hair miniaturized torsional actuator is capable of twisting 15000º and 590 revolutions/minute.

Zhou et al. produced a U-shape actuator using super-aligned CNTs which is capable of exhibiting large deformations such as 700º of twisting, 49.2 % of elongation, and 26.4 % diameter constriction.[198] The lightweight actuator, which uses electrothermal actuation, can produce a gripping force of 26 times higher than its own weight making it suitable for biomimetic devices.

5.2.6 Electrochemical devices

The electrochemical property of CNTs can be attributed to the distortion of electron clouds of CNTs from a uniform distribution to asymmetric distribution around the nanotubes caused by rich π-electron conjugation forms outside of CNTs.[199] As such, CNTs are extremely sensitive to charge transfer and doping effect by various molecules. Aligned CNTs arrays have been extensively used as electrochemical devices due to the high surface-area-to-volume ratio of the CNTs. The use of aligned CNTs arrays provides added benefit for a maximum access of CNTs electrode surface.[200] Chemical functionalization of CNTs can make CNTs sensitive to detect different analytes such as gas,[199] DNA,[200] protein,[201] neurochemical,[202] and biomolecules.[203] The key challenge in the fabrication of aligned CNTs arrays for electrochemical devices is to maintain the CNTs alignment structure in the array.[200] One way to protect the alignment structure is by filling the gaps between the aligned nanotubes with a spin-on-glass (SOG) prior to the oxidative reaction.[203] Another way would be using

self-assembly method to align the oxidized carbon nanotubes.[201] In both cases, however, the chemical attachment can only be done at the tip of the CNTs. He et. al. developed a method for preparing aligned CNTs with chemical attachment at both tip and side walls for CNTs via acid-plasma treatment, grafting and hybridization treatment.[200] As this paper is only intended to discuss the fabrication process and the potential of aligned CNTs, the performance of the electrochemical devices will not be discussed here. However, the readers are encouraged to refer to the review articles by Gao et al., Jacobs et al., Wang et al., Gooding et al., and Vashist et al. for more information about the performance of different electrochemical devices.[202-204]

5.3 Filters for purification

Carbon nanotubes membrane is a suitable candidate for filters for purification of water and gas due to its unique cylindrical nanostructure, high mechanical strength, high aspect ratio, and large surface area-volume ratio.[205] By the same token, CNTs membrane is also suitable for analytical separations such as selective separation of nanoparticles, biomolecules, or microorganism.[206] The keys to achieving good purifications using carbon nanotube membranes are the controlled porosity and pore size. Generally, 2 types of CNTs membranes are used as filters as purification, which is 1) bucky papers and 2) isoporous membranes (**figure 13**).

Generally, the aligned Bucky papers membranes are can be fabricated through domino-pushing of VA-CNTs or aligned magnetically. The CNTs in the Bucky papers are held together by the strong van der Waal's force to form a cohesive Bucky paper. It has been shown that longer carbon nanotube with fewer walls tends to exhibit better tensile property due to the stronger van der Waal's interaction. The Bucky papers of MWNT fabricated from domino pushing or lateral shear method (Figure 6b) of VA-CNTs with average outer diameter and length of 9 nm and 300 µm is found to have a pore size of ~25 nm and a standard deviation of ~14 nm. The porosity of Bucky paper is found be to around 87-91 % with finer CNTs having a higher porosity. A specific surface area of 1587 m^2

g^{-1} for Bucky-papers formed from SWNTs has been reported.[207] Bucky paper with high porosity (~90 %) has been reported to have water vapor permeability of up to 3.3×10^{-12} kg m^{-1} s^{-1} Pa^{-1} on a small scale rig.[208] PVDF can be added to the Bucky paper to reduce the chance of cracking at the expense of reduced flux and permeability.[208b] Besides, Bucky paper can be used as fine filters to remove 100-500 nm fine particle to a level that surpasses the standard HEPA filters.[209] Apart from that, Bucky paper has been reported capable of effectively filtering off E.coli bacteria (2 µm) and model virus MS2 bacteriophage (27 nm diameter).[210]

Unlike Bucky paper which uses the pores formed among the nanostructure to selectively allow particle (gas or water) to pass through, Isoporous membrane uses the cylindrical pore of CNTs to selectively allow molecules to pass through the hollow CNTs interior.[211] Generally, the isoporous membrane is fabricated in 2 steps, which are 1) growth of VA-CNTs and 2) infiltration of impermeable materials. Normally, the forest of VA-CNTs is first grown by CVD process with proper parameters, catalysts and substrates to avoid structural blockage which could prevent flow through the CNTs interior.[212] The VA-CNTs is then infiltrated with impermeable matrix material with low viscosity to ensure a void-free matrix and maintain the CNTs alignment.[205] Typically, the porosity for the isoporous membrane of 10^{11} cm^{-2} VA-CNTs forest and diameter of 5nm is roughly 2 %. Densification of VA-CNTs array is required to improve the permeation.[213] It has been shown that isoporous membrane of VA-CNTs of CNTs diameter (2 nm) can provide better gas permeance than the commercial polycarbonate membrane with 10 nm cylindrical pores.[212a]

5.4 Super-hydrophobic surface

Hydrophobicity refers to the ability of a surface to repel water molecules. CNTs are slightly hydrophilic with a contact angle of approximately 86º by nature. However, with VA-CNTs, the wettability changes from hydrophilic to hydrophobic, or even super-hydrophobic surface depending on the surface texture (**figure 14**).[214] Generally, the factors affecting the wettability of a surface are

the surface energy and surface texture/roughness. For the case of aligned CNTs, a stable hydrophobic surface can be achieved by using chemically modified VA-CNTs and micropatterned VA-CNTs. Chemically modified VA-CNTs are normally coated with a layer of fluorinated and silane (both are low surface energy compounds) to give the VA-CNTs the ability to have better water repelling property (contact angle: 171º). VA-CNTs with tunable wettability can be achieved by using thermoresponsive coating such as Poly(N-isopropylacrylamide) (PNIPAAm).[215] Besides, the super-hydrophobic surface can be achieved by ensuring the intertubular spacing is less than 50 µm.[216] For micropatterned VA-CNTs with anisotropic morphology, the water can be made to flow in a preferential direction.[217] The super-hydrophobicity of VA-CNTs is useful for applications such as loss-less transportation for microfluid and biological application such as cell seeding.[214]

6. CNTs meet 3D printing

6.1 Incorporation with various 3D printing techniques

In this section, the use of CNTs and its composite in 3D printing and the application of the 3D printed CNTs-based devices and structures are discussed. 3D Printing, also known as additive manufacturing, is a class of manufacturing techniques whereby the products are fabricated layer-by-layer in an additive manner.[218] It gives designers the flexibility to decide where and what materials to use when designing products because of the capability of 3D printing techniques to deposit/process the raw materials on demand. This allows added functionality to the products such as the selective strengthening of a structure or making certain parts of the structure conductive for specific applications. Currently, there are 4 types of 3D printing technique have been reported to have successfully fabricated CNTs-based devices or structures, namely material-extrusion technique, vat-polymerization technique, powder-bed fusion technique, and material-jetting technique.

6.1.1 Material-extrusion technique

Material-extrusion technique is a printing technique that lays/ deposits the materials in the form of filaments by forcing the feedstock materials through a nozzle (**figure 7a**). Generally, the feedstock materials used in the extrusion-based process are CNTs-composite either in solid filament[219] or in viscous liquid form[220]. During the extrusion process, the solid filaments are first melted to allow the materials to flow through the nozzle easily. On the contrary, heating is not required for feedstock materials in viscous liquid form. The extruded filament turns solid, either by solidification process for solid filament[219, 221] or UV-curing process and solvent casting process for viscous liquid feedstock,[220, 222] after exiting the nozzle. For solid filaments, Aliheidari et al. have demonstrated printing polyurethane/MWNT composite filament with an MWNTs of 1-3 w%.[222] For liquid feedstock materials, the materials must possess shear-thinning property to allow extrusion[223] and the particle size or CNTs length must be lower than 1/100 of the radius of the nozzle to prevent clogging of the nozzle.[224] Postiglione et al have shown that increasing CNTs concentration to about 35 % in the feedstock material increases the shear rate and thereby reducing the process window of the extrusion process.[222] To date, nanocomposite materials with matrix material of alginate [225], Poly (ε-caprolactone) (PCL),[226] acrylonitrile-butadiene-styrene (ABS).[219a] poly(lactic acid) (PLA),[222] and polyurethane[220] have been successfully fabricated using extrusion technique. As the extrusion process involves viscous materials flowing through a nozzle, extrusion-induced shear flow is developed in the extruding composite materials which allows the CNTs to redistribute and reorient themselves. As a result, preferential alignment of CNTs along the extrusion direction can be expected[219a, 223, 226-227]. To date, extrusion-based technique has been used to fabricate structural parts,[219a] liquid sensor,[219b] free standing circuit,[222] and tissue scaffold.[228]

6.1.2 Vat-polymerization technique

Vat-polymerization technique is a printing technique that selectively cures the liquid resin in the vat onto the build part. This method is more commonly known as stereolithography (SLA). A UV

laser source is used to cure the photocurable liquid resin. The use of CNTs in the liquid resin feedstock material is to overcome the shortcomings of the pure UV-curable polymer such as brittle, lack of strength and conductivity.[229] CNTs with average length between 1-20 µm have been shown suitable for SLA printing process.[230] Wagner has shown that the toughness of the printed nanocomposite is 11.4 w% higher than the pure counterpart by adding 0.25 w% of MWNT,[230] whereas Sandoval et al. have shown that the fracture stress of the printed nanocomposite is increased by 33 % by adding 0.1 w% of MWNT.[231] Yang et al. have demonstrated printing polymer/MWNT composite with controllable direction of CNTs (**figure 15**).[232] They added a pair of parallel-plate electrodes in the liquid resin tank to align the CNTs along the electric field direction. Besides, a rotatable build platform is used to turn the part into the desired orientation relative to the electric field in order to control the CNTs direction. They have shown that different mechanical property such as tensile modulus within a printed part is possible by controlling the orientation of the CNTs using this system.

6.1.3 Powder-bed fusion technique

Powder-bed fusion technique is a printing technique that uses laser to selectively fuse/sinter the powder feedstock material on the build platform (**figure 16**). Polymer nanocomposite parts such as polyamide (PA)/CNTs are normally fabricated from PA powder coated with CNTs of length range between 10-30 µm.[233] Yuan et al. have demonstrated printing the nanocomposite powder with 0.5 w% of CNTs using a selective laser sintering (SLS) printer. They have shown that the printed nanocomposite parts have improved the tensile strength and toughness of about 31.8 % and 84.9 % respectively as compared to the pure PA parts. However, current printing technique does not allow or promote alignment of CNTs, therefore it produces parts with random CNTs network.

6.1.4 Material-jetting technique

Material-jetting technique is a printing technique that deposit the ink in the form of droplet through a fine capillary (**figure 8b**). Among the material-jetting techniques, droplet-jetting technique

such as inkjet printing[122, 234] and aerosol jet[235] printing are a more popular options for printing high-resolution features of CNTs thin film for printed electronics. Unlike inkjet printing, aerosol jet printing is a 5-axis printer which allows features to be printed on any arbitrary surface topology. Both inkjet printing and aerosol jet techniques have similar requirement for the CNTs ink property. For droplet-jetting technique, the surface tension (30 mN m^{-1} and the viscosity (2 cP) of the CNTs ink have to be low in for good printability.[236] Similar to extrusion technique, the particle size or CNTs length depends on the diameter of the nozzle size. Typically, the dispersion of CNTs used for droplet-jetting technique normally have a concentration of around 0.5 w% with CNTs length as long as 2.6 µm.[122] Once the CNTs ink is patterned on the substrate, the patterned CNTs ink is left dried by either at room temperature or elevated temperature. With proper choice of CNTs concentration and evaporation rate, alignment of CNTs on the printed film can be achieved.[123] Alternatively, the CNTs can be aligned by utilizing the "coffee ring effect" of the printed film in which the CNTs is aligned along the printed film's boundary. To date, many electronic devices such as flexible circuits,[237] sensors,[238] transistors,[239] and flexible display[240] have been fabricated using droplet-jetting techniques.

Table 2 summarizes the relationship of the respective 3D printing techniques and the possibility of fabricating aligned CNTs devices.

Table 2. 3D Printing and the alignment of CNTs via 3D printing

3D Printing techniques	Alignment mechanisms	Advantages	Disadvantages	References
Material-extrusion	Shear flow-assisted	• Suitable for solid and liquid materials • 3D object • CNT alignment is possible • Suitable for nanocomposite	• In-plane alignment only • Not suitable for printing pure CNTs structures	[219a, 223, 226-227]
Vat-polymerization	Electric field-assisted	• 3D object • CNT alignment is possible • Controllable alignment direction	• In-plane alignment only • Not suitable for printing pure CNTs structure.	[232]

		• Suitable for nanocomposite materials		
Powder-bed fusion	-	• 3D object	• Random CNT orientation	[233]
Material-jetting	Self-assembly	• Simple • High resolution • CNT alignment is possible • Suitable for printing pure CNTs	• 2D thin film • In-plane alignment only	[123]

6.2 Potential of 3D printed CNTs structures and devices

6.2.1 Various applications of 3D printed CNTs and its composite

3D printed CNT-based devices or structures can be used in many fields such as mechanical structure, robotics, electronics, optoelectronics and bioengineering fields. For instance, Yang et al. demonstrated the unconventional design flexibility of 3D printing by fabricating a CNTs-reinforced medial meniscus with controlled tensile modulus at different region of the meniscus.[232] Besides, Zarek et al. have demonstrated a 3D printed shape memory polymer with CNTs showing the possibility for these devices to be applied as actuators for soft robotics.[241] In addition, the biocompatibility of CNTs-alginate composite have been shown useful for application such as tissue scaffolds.[228] Nonetheless, CNTs, being an electrically conductive materials, have been applied widely to fabricate many kinds of electronics devices. For examples, Postiglione et al. have demonstrated fabrication of free-standing electrical circuit utilizing a freeform prototyping tool.[222] Passive and active electrical components such as micro-supercapacitor and transistors have been fabricated via 3D printing.[242] Many types of CNTs-based sensor such as strain sensor,[243] pH sensor,[238a] liquid sensor,[219b] chemical sensor[244] and etc. have been printed and tested. Besides, optoelectronics devices such as electroluminescent[236a] and flexible display[240] have been shown possible to be fabricated using 3D printing. Here, it is easy to see that the usefulness of 3D printing

and the flexibility of these tools to be adapted with various fields to fabricate different devices with added functionality.

6.2.2 Miniaturization of electronic devices

Currently, most of the 3D printing techniques for electronics fabrication can achieve high print resolution which advantageous for the fabrication of high-performance electronics. For instance, inkjet printing process has a reported print resolution of around 30 µm, whereas aerosol jet printing has been reported to achieve a resolution as low as 10 µm.[245] With high print resolution, miniaturization of electronic devices is made possible by reducing the size of each electronic component. For example, Goh et al. have fabricated a CNTs-based pH sensor with a serpentine sensing element and a line width as low as 20 µm using aerosol jet printing.[238a] The chemiresistive pH sensor exhibits high sensitivity (up to 59 kΩ/pH) and repeatability (coefficient of variance <1.15 %) with a response time of 20 s. Besides, Li et al. have fabricated a high sensitivity strain gauge with a gauge factor as high as 40 by using aligned CNTs film with printed microelectrodes of gap resolution of 30 µm using aerosol jet printing technique.[70] In addition, miniaturization is one of the key factor to improving the performance of transistor in terms of speed.[246] Ha et al. fabricated an aerosol jet printed CNTs-based transistor with a channel length of 10 um, channel width of 100 um and a thickness of 1.2 µm.[247] The transistor showed superior high electron and hole mobilities (~20 cm^2 $(V\ s)^{-1}$) and ON/OFF current ratios (up to 10^5). Hence, it is clear that the miniaturization of electronic devices is essential for high-performance electronics with improved sensitivity and speed.

6.2.3 Hybrid construct for wearables

Wearable electronic devices are electronic systems that can be worn by human either to monitor or to aid in daily activities.[248] As such, these wearables are normally made to match the skin's property such as flexibility and stretchability for additional comfort. CNTs, being a conductive

material that is flexible and can be made stretchable in some condition, is a good candidate to be used as functional ink for wearable devices.[249] However, the commonly used substrates that are flexible such as polyimide or stretchable such as PDMS are unsuitable to be processed using the conventional PCB manufacturing technique.[248] On the contrary, 3D printing techniques such as inkjet printing and aerosol jet printing techniques, which are more adaptable in terms of the choice of the substrate materials, can be used to process these kinds of materials.[249] In particular, aerosol jet printing technique can be used print the antenna and electronic circuit directly onto the device enclosure such as hearing aid and molded interconnect device (MID).[250] These hybrid constructs do not only reduce the device dimension and weight by eliminating the use of printed circuit board (PCB), but it also adds functionality to the devices structure and improves the product's overall user experience. For example, textile can have added functionality by printing the CNTs ink directly on to the textile surface without the need of PCB.[251] Till now, CNTs-based wearable sensors have seen many applications in healthcare, motion detection and environmental probing.[252] Among those CNTs-based wearables, 3D printed wearable devices that have been demonstrated are supercapacitor,[253] strain sensor,[254] motion sensor,[255] chemical vapor sensing system,[255-256] and transistor.[257] In addition, bioactive CNTs ink can be used to fabricate biocompatible 2D or 3D hybrid tissue construct with good electrical property for monitoring application.[258]

7. Conclusion & Outlook

This review highlights the fact that there are many possible mechanisms for aligning carbon nanotubes. Here, the focus is on the working principle and the underlying mechanism of fabricating aligned CNTs devices, either from in-situ method or ex-situ method.

This review has categorized the existing developed techniques into 9 different groups: (1) electrostatic and van der Waals forces- induced alignment, (2) magnetic-field induced alignment, (3)

electric-field induced alignment, (4) strain-induced alignment, (5) shear-induced alignment, (6) extrusion-induced alignment, (7) fluid flow-induced alignment, (8) self-assembly and liquid crystal-induced method, and (9) surface acoustic wave-induced alignment. Undeniably, some techniques can fall into multiple categories and to create a clear boundary between categories is almost impossible. However, the classifications are still helpful in understanding the key drivers of CNTs alignment.

Apart from that, this review has discussed the potential applications and properties of aligned CNTs devices. The reviewed applications include composite materials, electronic devices, purification, and super-hydrophobic surface. In particular, the material properties such as the mechanical, electrical and thermal property of the composite has been discussed. Also, various electronic devices such as electrodes for energy storage devices, field emission devices, field-effect transistor, optoelectronics, electromechanical devices, and electrochemical devices have been discussed.

Despite the advancement in the CNTs alignment techniques, there are still several challenges that remain to be addressed. For instance, the fabrication of aligned CNTs with controlled diameter and chirality using CVD techniques remains a big challenge as an additional step of CNTs separation is required to remove metallic CNTs.[259] Current metallic removal method such as plasma etching and light irradiation would bring defects to the remaining semiconducting CNTs. Besides, most techniques do not work well with a high packing density of CNTs due to the strong randomizing inter-nanotube interactions resulting in CNTs misalignment.[26] For the post-fabrication CNTs, the 2 main challenges are (1) the tendency of the CNTs to form aggregates and (2) the insolubility in common organic solvent.[112c]

In short, many CNTs alignment techniques have been developed and aligned CNTs devices have been widely used in various fields. Future work on CNTs alignment should be focusing on developing techniques that are scalable and can be integrated into existing fabricating processes such

as 3D printing, as well as to address the current challenges mentioned above. As this research area continues to mature, undiscovered CNTs aligning mechanisms will be revealed and newer approaches will be developed leading towards the ultimate manipulation and alignment of CNTs.

Conflicts of interest

The authors confirm that there are no known conflicts of interest associated with this publication and there has been no significant financial support for this work that could have influenced its outcome

Acknowledgements

This research is supported by the National Research Foundation, Prime Minister's Office, Singapore under its Medium-Sized Centre funding scheme.

Received: ((will be filled in by the editorial staff))
Revised: ((will be filled in by the editorial staff))
Published online: ((will be filled in by the editorial staff))

References

[1] G. Eres, C. Rouleau, A. Puretzky, D. Geohegan, H. Wang, *Phys. Rev. Appl.*, **2018**, *10*, 024010.
[2] K. Liu, Y. Sun, L. Chen, C. Feng, X. Feng, K. Jiang, Y. Zhao, S. Fan, *Nano Lett.*, **2008**, *8*, 700.
[3] X. Zhang, A. Cao, Y. Li, C. Xu, J. Liang, D. Wu, B. Wei, *Chem. Phys. Lett.*, **2002**, *351*, 183.
[4] F.N. Ishikawa, H.-k. Chang, K. Ryu, P.-c. Chen, A. Badmaev, L. Gomez De Arco, G. Shen, C. Zhou, *ACS nano*, **2008**, *3*, 73.
[5] R. Rahman, P. Servati, *Nanotechnology*, **2012**, *23*, 055703.
[6] E.T. Thostenson, T.-W. Chou, *Journal of physics D: Applied physics*, **2002**, *35*, L77.
[7] G. Yu, A. Cao, C.M. Lieber, *Nat. Nanotechnol.*, **2007**, *2*, 372.
[8] R.F. Rajter, R. Podgornik, V.A. Parsegian, R.H. French, W. Ching, *Phys. Rev. B*, **2007**, *76*, 045417.
[9] A. Ramirez, R. Haddon, R. Zhou, *Nucl. Magn. Reson. (NMR)*, **1994**, *8*, 9.
[10] E. Minot, Y. Yaish, V. Sazonova, P.L. McEuen, *Nature*, **2004**, *428*, 536.
[11] M. Fujiwara, E. Oki, M. Hamada, Y. Tanimoto, I. Mukouda, Y. Shimomura, *The Journal of physical chemistry A*, **2001**, *105*, 4383.
[12] C. Kamal, T. Ghanty, A. Banerjee, A. Chakrabarti, *The Journal of chemical physics*, **2009**, *131*, 164708.
[13] a) S. Botti, A. Castro, X. Andrade, A. Rubio, M.A. Marques, *Phys. Rev. B*, **2008**, *78*, 035333; b) J. Lennard-Jones, *Trans. Faraday Soc.*, **1932**, *28*, 333; c) I. Lifshitz, A. Kosevich, *English translation 1956 Soviet Phys. JETP*, **1955**, *2*, 636; d) E. Zaremba, W. Kohn, *Phys. Rev. B*, **1977**, *15*, 1769.
[14] A. Šiber, R. Rajter, R. French, W. Ching, V. Parsegian, R. Podgornik, *Phys. Rev. B*, **2009**, *80*, 165414.
[15] A. Oliva-Avilés, F. Avilés, V. Sosa, A. Oliva, F. Gamboa, *Nanotechnology*, **2012**, *23*, 465710.
[16] a) M. Dimaki, P. Bøggild, *Nanotechnology*, **2004**, *15*, 1095; b) M.P. Hughes, *Nanotechnology*, **2000**, *11*, 124.

[17] M. Cavallaro, L. Botto, E.P. Lewandowski, M. Wang, K.J. Stebe, *Proc. Natl. Acad. Sci.*, **2011**, *108*, 20923.
[18] H. Zeng, K. Kristiansen, P. Wang, J. Bergli, J. Israelachvili, *Langmuir*, **2011**, *27*, 7163.
[19] G. Lu, K. Yu, J. Chen, *J. Nanosci. Nanotechnol.*, **2012**, *12*, 6968.
[20] R.S. Mclean, X. Huang, C. Khripin, A. Jagota, M. Zheng, *Nano Lett.*, **2006**, *6*, 55.
[21] W.P. Lim, K. Yao, Y. Chen, *The Journal of Physical Chemistry C*, **2007**, *111*, 16802.
[22] K. Darowicki, A. Zieliński, K.J. Kurzydłowski, *Sci. Technol. Adv. Mater.*, **2008**, *9*, 045006.
[23] P. Gupta, S. Sharan, P. Roy, D. Lahiri, *Carbon*, **2015**, *95*, 715.
[24] D. Fujita, K. Sagisaka, *Sci. Technol. Adv. Mater.*, **2008**, *9*, 013003.
[25] J.M. Russell, S. Oh, I. LaRue, O. Zhou, E.T. Samulski, *Thin Solid Films*, **2006**, *509*, 53.
[26] M.T. Cole, V. Cientanni, W.I. Milne, *Nanoscale*, **2016**, *8*, 15836.
[27] A. Jorio, M. Pimenta, A. Souza Filho, R. Saito, G. Dresselhaus, M. Dresselhaus, *New J. Phys.*, **2003**, *5*, 139.
[28] S. Li, J.G. Park, Z. Liang, T. Siegrist, T. Liu, M. Zhang, Q. Cheng, B. Wang, C. Zhang, *Carbon*, **2012**, *50*, 3859.
[29] S. Gbordzoe, S. Yarmolenko, Y.-Y. Hsieh, P.K. Adusei, N.T. Alvarez, S. Fialkova, V. Shanov, *Carbon*, **2017**, *121*, 591.
[30] a) X. Ke, S. Bals, D. Cott, T. Hantschel, H. Bender, G. Van Tendeloo, *Microsc. Microanal.*, **2010**, *16*, 210; b) B. Natarajan, N. Lachman, T. Lam, D. Jacobs, C. Long, M. Zhao, B.L. Wardle, R. Sharma, J.A. Liddle, *ACS nano*, **2015**, *9*, 6050.
[31] Z. Ren, Y. Lan, Y. Wang, *Aligned carbon nanotubes: physics, concepts, fabrication and devices*, Springer Science & Business Media**2012**.
[32] K. Iakoubovskii, *Cent. Eur. J. Phys.*, **2009**, *7*, 645.
[33] G. Zhang, D. Mann, L. Zhang, A. Javey, Y. Li, E. Yenilmez, Q. Wang, J.P. McVittie, Y. Nishi, J. Gibbons, *Proceedings of the National Academy of Sciences of the United States of America*, **2005**, *102*, 16141.
[34] S. Fan, M.G. Chapline, N.R. Franklin, T.W. Tombler, A.M. Cassell, H. Dai, *Science*, **1999**, *283*, 512.
[35] S. Chakrabarti, T. Nagasaka, Y. Yoshikawa, L. Pan, Y. Nakayama, *Japanese journal of applied physics*, **2006**, *45*, L720.
[36] W. Li, S. Xie, L. Qian, B. Chang, *Science*, **1996**, *274*, 1701.
[37] J.S. Suh, J.S. Lee, *Appl. Phys. Lett.*, **1999**, *75*, 2047.
[38] a) N. Wang, Z.-K. Tang, G.-D. Li, J. Chen, *Nature*, **2000**, *408*, 50; b) R.C. Smith, W.M. Fischer, D.L. Gin, *J. Am. Chem. Soc.*, **1997**, *119*, 4092.
[39] A.K. Sinha, D.W. Hwang, L.-P. Hwang, *Chem. Phys. Lett.*, **2000**, *332*, 455.
[40] L. Dai, A. Patil, X. Gong, Z. Guo, L. Liu, Y. Liu, D. Zhu, *ChemPhysChem*, **2003**, *4*, 1150.
[41] L. Zhu, Y. Xiu, D.W. Hess, C.-P. Wong, *Nano Lett.*, **2005**, *5*, 2641.
[42] G.D. Nessim, D. Acquaviva, M. Seita, K.P. O'brien, C.V. Thompson, *Adv. Funct. Mater.*, **2010**, *20*, 1306.
[43] D.N. Futaba, K. Hata, T. Namai, T. Yamada, K. Mizuno, Y. Hayamizu, M. Yumura, S. Iijima, *The Journal of Physical Chemistry B*, **2006**, *110*, 8035.
[44] P. Diao, Z. Liu, *Adv. Mater.*, **2010**, *22*, 1430.
[45] a) T. El-Aguizy, S.-G. Kim, "Large-scale assembly of carbon nanotubes", presented at *ASME 2004 3rd Integrated Nanosystems Conference*, **2004**; b) Y. Wang, D. Maspoch, S. Zou, G.C. Schatz, R.E. Smalley, C.A. Mirkin, *Proceedings of the National Academy of Sciences of the United States of America*, **2006**, *103*, 2026.
[46] X. Cao, F. Wu, C. Lau, Y. Liu, Q. Liu, C. Zhou, *ACS nano*, **2017**, *11*, 2008.

[47] a) N. Kumar, W. Curtis, J.-i. Hahm, *Appl. Phys. Lett.*, **2005**, *86*, 173101; b) K.-H. Lee, J.-M. Cho, W. Sigmund, *Appl. Phys. Lett.*, **2003**, *82*, 448.
[48] a) J. Hone, M. Llaguno, N. Nemes, A. Johnson, J. Fischer, D. Walters, M. Casavant, J. Schmidt, R. Smalley, *Appl. Phys. Lett.*, **2000**, *77*, 666; b) J.P. Lu, *Phys. Rev. Lett.*, **1995**, *74*, 1123.
[49] a) E. Choi, J. Brooks, D. Eaton, M. Al-Haik, M. Hussaini, H. Garmestani, D. Li, K. Dahmen, *J. Appl. Phys.*, **2003**, *94*, 6034; b) H. Garmestani, M.S. Al‐Haik, K. Dahmen, R. Tannenbaum, D. Li, S.S. Sablin, M.Y. Hussaini, *Adv. Mater.*, **2003**, *15*, 1918; c) B.W. Steinert, D.R. Dean, *Polymer*, **2009**, *50*, 898; d) T. Kimura, H. Ago, M. Tobita, S. Ohshima, M. Kyotani, M. Yumura, *Adv. Mater.*, **2002**, *14*, 1380; e) Y. He, S. Yang, H. Liu, Q. Shao, Q. Chen, C. Lu, Y. Jiang, C. Liu, Z. Guo, *J. Colloid Interface Sci.*, **2018**, *517*, 40.
[50] J. Shaver, A.N.G. Parra-Vasquez, S. Hansel, O. Portugall, C.H. Mielke, M. Von Ortenberg, R.H. Hauge, M. Pasquali, J. Kono, *ACS nano*, **2008**, *3*, 131.
[51] a) B. Smith, Z. Benes, D. Luzzi, J. Fischer, D. Walters, M. Casavant, J. Schmidt, R. Smalley, *Appl. Phys. Lett.*, **2000**, *77*, 663; b) J.E. Fischer, W. Zhou, J. Vavro, M.C. Llaguno, C. Guthy, R. Haggenmueller, M. Casavant, D. Walters, R.E. Smalley, *J. Appl. Phys.*, **2003**, *93*, 2157.
[52] M. Abdalla, D. Dean, M. Theodore, J. Fielding, E. Nyairo, G. Price, *Polymer*, **2010**, *51*, 1614.
[53] a) K. Kordás, T. Mustonen, G. Tóth, J. Vähäkangas, A. Uusimäki, H. Jantunen, A. Gupta, K. Rao, R. Vajtai, P.M. Ajayan, *Chem. Mater.*, **2007**, *19*, 787; b) G. Korneva, H. Ye, Y. Gogotsi, D. Halverson, G. Friedman, J.-C. Bradley, K.G. Kornev, *Nano Lett.*, **2005**, *5*, 879.
[54] K. Iakoubovskii, *Open Phys.*, **2009**, *7*, 645.
[55] P. Poulin, B. Vigolo, P. Launois, *Carbon*, **2002**, *40*, 1741.
[56] J. Wen, Z. Huang, D. Wang, J. Chen, S. Yang, Z. Ren, J. Wang, L. Calvet, J. Chen, J. Klemic, *Journal of Materials Research*, **2001**, *16*, 3246.
[57] a) Y. Gao, Y. Zhou, W. Xiong, M. Mahjouri-Samani, M. Mitchell, Y. Lu, *Appl. Phys. Lett.*, **2009**, *95*, 143117; b) A. Nojeh, A. Ural, R.F. Pease, H. Dai, *J. Vac. Sci. Technol., B: Microelectron. Nanometer Struct.--Process., Meas., Phenom.*, **2004**, *22*, 3421.
[58] C. Bower, O. Zhou, W. Zhu, D. Werder, S. Jin, *Appl. Phys. Lett.*, **2000**, *77*, 2767.
[59] Y. Shiratori, H. Hiraoka, Y. Takeuchi, S. Itoh, M. Yamamoto, *Appl. Phys. Lett.*, **2003**, *82*, 2485.
[60] Y.C. Choi, Y.M. Shin, Y.H. Lee, B.S. Lee, G.-S. Park, W.B. Choi, N.S. Lee, J.M. Kim, *Appl. Phys. Lett.*, **2000**, *76*, 2367.
[61] Y. Hayashi, T. Negishi, S. Nishino, *J. Vac. Sci. Technol., A*, **2001**, *19*, 1796.
[62] T. Minea, S. Point, A. Gohier, A. Granier, C. Godon, F. Alvarez, *Surf. Coat. Technol.*, **2005**, *200*, 1101.
[63] a) J. Ramón‐Azcón, S. Ahadian, M. Estili, X. Liang, S. Ostrovidov, H. Kaji, H. Shiku, M. Ramalingam, K. Nakajima, Y. Sakka, *Adv. Mater.*, **2013**, *25*, 4028; b) S. Ahadian, J. Ramón-Azcón, M. Estili, X. Liang, S. Ostrovidov, H. Shiku, M. Ramalingam, K. Nakajima, Y. Sakka, H. Bae, *Sci. Rep.*, **2014**, *4*, 4271.
[64] Y.-F. Zhu, C. Ma, W. Zhang, R.-P. Zhang, N. Koratkar, J. Liang, *J. Appl. Phys.*, **2009**, *105*, 054319.
[65] X. Liu, J.L. Spencer, A.B. Kaiser, W.M. Arnold, *Current Applied Physics*, **2004**, *4*, 125.
[66] X. Chen, T. Saito, H. Yamada, K. Matsushige, *Appl. Phys. Lett.*, **2001**, *78*, 3714.
[67] S.U. Khan, J.R. Pothnis, J.-K. Kim, *Composites, Part A*, **2013**, *49*, 26.
[68] K. Yamamoto, S. Akita, Y. Nakayama, *Journal of physics D: Applied physics*, **1998**, *31*, L34.
[69] M. Frogley, Q. Zhao, H. Wagner, *Phys. Rev. B*, **2002**, *65*, 113413.
[70] S. Li, J.G. Park, S. Wang, R. Liang, C. Zhang, B. Wang, *Carbon*, **2014**, *73*, 303.
[71] a) L. Jiang, C. Nath, J. Samuel, S.G. Kapoor, *Trans. ASME, Ser. B*, **2015**, *137*, 021009; b) L. Jin, C. Bower, O. Zhou, *Appl. Phys. Lett.*, **1998**, *73*, 1197.

[72] S. Shang, W. Zeng, X.-m. Tao, *Journal of Materials Chemistry*, **2011**, *21*, 7274.
[73] A.R. Bhattacharyya, T. Sreekumar, T. Liu, S. Kumar, L.M. Ericson, R.H. Hauge, R.E. Smalley, *Polymer*, **2003**, *44*, 2373.
[74] S. Badaire, V. Pichot, C. Zakri, P. Poulin, P. Launois, J. Vavro, C. Guthy, M. Chen, J.E. Fischer, *J. Appl. Phys.*, **2004**, *96*, 7509.
[75] F. Du, J.E. Fischer, K.I. Winey, *Physical Review B*, **2005**, *72*, 121404.
[76] Y.-L. Li, I.A. Kinloch, A.H. Windle, *Science*, **2004**, *304*, 276.
[77] X. Zhang, K. Jiang, C. Feng, P. Liu, L. Zhang, J. Kong, T. Zhang, Q. Li, S. Fan, *Adv. Mater.*, **2006**, *18*, 1505.
[78] L. Zhang, X. Wang, W. Xu, Y. Zhang, Q. Li, P.D. Bradford, Y. Zhu, *Small*, **2015**, *11*, 3830.
[79] W. Xiong, Y. Liu, L.J. Jiang, Y.S. Zhou, D.W. Li, L. Jiang, J.F. Silvain, Y.F. Lu, *Adv. Mater.*, **2016**, *28*, 2002.
[80] P. Ajayan, O. Stephan, C. Colliex, D. Trauth, *Science-AAAS-Weekly Paper Edition*, **1994**, *265*, 1212.
[81] W.A. de Heer, W. Bacsa, A. Chatelain, T. Gerfin, R. Humphrey-Baker, *Science*, **1995**, *268*, 845.
[82] L.J. Lanticse, Y. Tanabe, K. Matsui, Y. Kaburagi, K. Suda, M. Hoteida, M. Endo, E. Yasuda, *Carbon*, **2006**, *44*, 3078.
[83] D. Wang, P. Song, C. Liu, W. Wu, S. Fan, *Nanotechnology*, **2008**, *19*, 075609.
[84] C.L. Pint, Y.-Q. Xu, S. Moghazy, T. Cherukuri, N.T. Alvarez, E.H. Haroz, S. Mahzooni, S.K. Doorn, J. Kono, M. Pasquali, *ACS nano*, **2010**, *4*, 1131.
[85] M. Miansari, A. Qi, L.Y. Yeo, J.R. Friend, *Adv. Funct. Mater.*, **2015**, *25*, 1014.
[86] H. Zhao, Z. Zhou, H. Dong, L. Zhang, H. Chen, L. Hou, *Sci. Rep.*, **2013**, *3*, 3480.
[87] S. Huang, C. Zhao, W. Pan, Y. Cui, H. Wu, *Nano Lett*, **2015**, *15*, 1609.
[88] M.M. Hossain, M.A. Islam, H. Shima, M. Hasan, M. Lee, *ACS Appl. Mater. Interfaces*, **2017**, *9*, 5530.
[89] R. Haggenmueller, H. Gommans, A. Rinzler, J.E. Fischer, K. Winey, *Chem. Phys. Lett.*, **2000**, *330*, 219.
[90] P. Pötschke, A.R. Bhattacharyya, A. Janke, S. Pegel, A. Leonhardt, C. Täschner, M. Ritschel, S. Roth, B. Hornbostel, J. Cech, *Fullerenes, Nanotubes, Carbon Nanostruct.*, **2005**, *13*, 211.
[91] B. Vigolo, A. Penicaud, C. Coulon, C. Sauder, R. Pailler, C. Journet, P. Bernier, P. Poulin, *Science*, **2000**, *290*, 1331.
[92] a) C. Jiang, A. Saha, C.C. Young, D.P. Hashim, C.E. Ramirez, P.M. Ajayan, M. Pasquali, A.A. Martí, *ACS nano*, **2014**, *8*, 9107; b) S. Zhang, K.K. Koziol, I.A. Kinloch, A.H. Windle, *Small*, **2008**, *4*, 1217.
[93] J.P. Lewicki, J.N. Rodriguez, C. Zhu, M.A. Worsley, A.S. Wu, Y. Kanarska, J.D. Horn, E.B. Duoss, J.M. Ortega, W. Elmer, *Scientific Reports*, **2017**, *7*.
[94] M. Inagaki, Y. Yang, F. Kang, *Adv. Mater.*, **2012**, *24*, 2547.
[95] F. Ko, Y. Gogotsi, A. Ali, N. Naguib, H. Ye, G. Yang, C. Li, P. Willis, *Adv. Mater.*, **2003**, *15*, 1161.
[96] F. Lionetto, E. Calò, F. Di Benedetto, D. Pisignano, A. Maffezzoli, *Compos. Sci. Technol.*, **2014**, *96*, 47.
[97] S. Huang, B. Maynor, X. Cai, J. Liu, *Adv. Mater.*, **2003**, *15*, 1651.
[98] S. Huang, Q. Fu, L. An, J. Liu, *Phys. Chem. Chem. Phys.*, **2004**, *6*, 1077.
[99] S. Huang, X. Cai, C. Du, J. Liu, *The Journal of Physical Chemistry B*, **2003**, *107*, 13251.
[100] a) S. Huang, M. Woodson, R. Smalley, J. Liu, *Nano Lett.*, **2004**, *4*, 1025; b) A. Reina, M. Hofmann, D. Zhu, J. Kong, *The Journal of Physical Chemistry C*, **2007**, *111*, 7292.
[101] S. Huang, X. Cai, J. Liu, *J. Am. Chem. Soc.*, **2003**, *125*, 5636.

[102] Z. Jin, H. Chu, J. Wang, J. Hong, W. Tan, Y. Li, *Nano Lett.*, **2007**, *7*, 2073.
[103] G. Hong, B. Zhang, B. Peng, J. Zhang, W.M. Choi, J.-Y. Choi, J.M. Kim, Z. Liu, *J. Am. Chem. Soc.*, **2009**, *131*, 14642.
[104] H. Xin, A.T. Woolley, *Nano Lett.*, **2004**, *4*, 1481.
[105] M.C. LeMieux, M. Roberts, S. Barman, Y.W. Jin, J.M. Kim, Z. Bao, *Science*, **2008**, *321*, 101.
[106] B. Safadi, R. Andrews, E. Grulke, *J. Appl. Polym. Sci.*, **2002**, *84*, 2660.
[107] Y. Wang, S.K.R. Pillai, M.B. Chan‐Park, *Small*, **2013**, *9*, 2960.
[108] R.H. Schmidt, I.A. Kinloch, A.N. Burgess, A.H. Windle, *Langmuir*, **2007**, *23*, 5707.
[109] a) Y. Yan, S. Li, L. Chen, M. Chan-Park, Q. Zhang, *Nanotechnology*, **2006**, *17*, 5696; b) P. Kim, S. Baik, K.Y. Suh, *Small*, **2008**, *4*, 92.
[110] J.M. Russell, S. Oh, I. LaRue, O. Zhou, E.T. Samulski, *Thin Solid Films*, **2006**, *509*, 53.
[111] a) S. Abbasi, P.J. Carreau, A. Derdouri, *Polymer*, **2010**, *51*, 922; b) R.D. Farahani, M. Pahlavanpour, H. Dalir, B. Aissa, M.A. El Khakani, M. Lévesque, D. Therriault, *Mater. Des.*, **2012**, *41*, 214.
[112] a) M.D. Lynch, D.L. Patrick, *Nano Lett.*, **2002**, *2*, 1197; b) I. Dierking, G. Scalia, P. Morales, *J. Appl. Phys.*, **2005**, *97*, 044309; c) I. Dierking, G. Scalia, P. Morales, D. LeClere, *Adv. Mater.*, **2004**, *16*, 865; d) G. Scalia, M. Haluska, U. Dettlaff‐Weglikowska, F. Giesselmann, S. Roth, H. Kuzmany, J. Fink, M. Mehring, S. Roth, "Polarized Raman spectroscopy study of SWCNT orientational order in an aligning liquid crystalline matrix", presented at *AIP Conference Proceedings*, **2005**.
[113] a) J. Lagerwall, G. Scalia, M. Haluska, U. Dettlaff‐Weglikowska, S. Roth, F. Giesselmann, *Advanced Materials*, **2007**, *19*, 359; b) J.P. Lagerwall, G. Scalia, M. Haluska, U. Dettlaff‐Weglikowska, F. Giesselmann, S. Roth, *physica status solidi (b)*, **2006**, *243*, 3046; c) V. Weiss, R. Thiruvengadathan, O. Regev, *Langmuir*, **2006**, *22*, 854; d) G. Scalia, C. von Bühler, C. Hägele, S. Roth, F. Giesselmann, J.P. Lagerwall, *Soft Matter*, **2008**, *4*, 570.
[114] W. Song, I.A. Kinloch, A.H. Windle, *Science*, **2003**, *302*, 1363.
[115] C. Zamora-Ledezma, C. Blanc, M. Maugey, C. Zakri, P. Poulin, E. Anglaret, *Nano Lett.*, **2008**, *8*, 4103.
[116] C. Zakri, *Liq. Cryst. Today*, **2007**, *16*, 1.
[117] M.E. Spotnitz, D. Ryan, H.A. Stone, *J. Mater. Chem.*, **2004**, *14*, 1299.
[118] T.J. Simmons, D. Hashim, R. Vajtai, P.M. Ajayan, *J. Am. Chem. Soc.*, **2007**, *129*, 10088.
[119] R. Picknett, R. Bexon, *J. Colloid Interface Sci.*, **1977**, *61*, 336.
[120] H.Z. Yu, D.M. Soolaman, A.W. Rowe, J.T. Banks, *ChemPhysChem*, **2004**, *5*, 1035.
[121] Q. Li, Y.T. Zhu, I.A. Kinloch, A.H. Windle, *The Journal of Physical Chemistry B*, **2006**, *110*, 13926.
[122] N.T. Dinh, E. Sowade, T. Blaudeck, S. Hermann, R.D. Rodriguez, D.R. Zahn, S.E. Schulz, R.R. Baumann, O. Kanoun, *Carbon*, **2016**, *96*, 382.
[123] S.T. Beyer, K. Walus, *Langmuir*, **2012**, *28*, 8753.
[124] M. Engel, J.P. Small, M. Steiner, M. Freitag, A.A. Green, M.C. Hersam, P. Avouris, *ACS nano*, **2008**, *2*, 2445.
[125] S.W. Hong, W. Jeong, H. Ko, M.R. Kessler, V.V. Tsukruk, Z. Lin, *Adv. Funct. Mater.*, **2008**, *18*, 2114.
[126] Y. Takagi, Y. Nobusa, S. Gocho, H. Kudou, K. Yanagi, H. Kataura, T. Takenobu, *Appl. Phys. Lett.*, **2013**, *102*, 143107.
[127] X. Li, L. Zhang, X. Wang, I. Shimoyama, X. Sun, W.-S. Seo, H. Dai, *J. Am. Chem. Soc.*, **2007**, *129*, 4890.
[128] K.M. Seemann, J. Ebbecke, A. Wixforth, *Nanotechnology*, **2006**, *17*, 4529.

[129] Z. Ma, J. Guo, Y.J. Liu, Y. Ai, *Nanoscale*, **2015**, *7*, 14047.
[130] C. Strobl, C. Schäflein, U. Beierlein, J. Ebbecke, A. Wixforth, *Appl. Phys. Lett.*, **2004**, *85*, 1427.
[131] C. Wood, S. Evans, J. Cunningham, R. O'Rorke, C. Wälti, A. Davies, *Appl. Phys. Lett.*, **2008**, *92*, 044104.
[132] T. Smorodin, U. Beierlein, J. Ebbecke, A. Wixforth, *Small*, **2005**, *1*, 1188.
[133] M. Su, Y. Li, B. Maynor, A. Buldum, J.P. Lu, J. Liu, *The Journal of Physical Chemistry B*, **2000**, *104*, 6505.
[134] S. Han, X. Liu, C. Zhou, *J. Am. Chem. Soc.*, **2005**, *127*, 5294.
[135] C. Kocabas, S.H. Hur, A. Gaur, M.A. Meitl, M. Shim, J.A. Rogers, *small*, **2005**, *1*, 1110.
[136] H. Ago, K. Nakamura, K.-i. Ikeda, N. Uehara, N. Ishigami, M. Tsuji, *Chem. Phys. Lett.*, **2005**, *408*, 433.
[137] A. Ismach, L. Segev, E. Wachtel, E. Joselevich, *Angew. Chem.*, **2004**, *116*, 6266.
[138] A. Ismach, D. Kantorovich, E. Joselevich, *J. Am. Chem. Soc.*, **2005**, *127*, 11554.
[139] S.-H. Lee, J. Park, H.-R. Kim, T. Lee, J. Lee, Y.-O. Im, C.-H. Lee, H. Cho, H. Lee, C.-H. Jun, *Carbon*, **2016**, *100*, 647.
[140] T. Yeshua, C. Lehmann, U. Hübner, S. Azoubel, S. Magdassi, E.E. Campbell, S. Reich, A. Lewis, *Nano Lett.*, **2016**, *16*, 1517.
[141] J. Hedberg, L. Dong, J. Jiao, *Appl. Phys. Lett.*, **2005**, *86*, 143111.
[142] K. Jiang, J. Wang, Q. Li, L. Liu, C. Liu, S. Fan, *Adv. Mater.*, **2011**, *23*, 1154.
[143] T. Ogasawara, S. Hanamitsu, T. Ogawa, S.-Y. Moon, Y. Shimamura, Y. Inoue, *Adv. Compos. Mater.*, **2017**, *26*, 157.
[144] Q. Cheng, J. Wang, J. Wen, C. Liu, K. Jiang, Q. Li, S. Fan, *Carbon*, **2010**, *48*, 260.
[145] P. Miaudet, S. Badaire, M. Maugey, A. Derre, V. Pichot, P. Launois, P. Poulin, C. Zakri, *Nano Lett.*, **2005**, *5*, 2212.
[146] X. Ni, E. Kalfon-Cohen, C. Furtado, R. Kopp, N.K. Fritz, A. Arteiro, G.A. Valdes, G. Borstnar, M. Mavrogordato, S. Spearing, "Interlaminar reinforcement of carbon fiber composites using aligned carbon nanotubes", presented at *submitted to the 21st International Conference on Composite Materials (ICCM), Xi'an, China*, **2017**.
[147] X. Wang, P.D. Bradford, W. Liu, H. Zhao, Y. Inoue, J.-P. Maria, Q. Li, F.-G. Yuan, Y. Zhu, *Compos. Sci. Technol.*, **2011**, *71*, 1677.
[148] P. Gonnet, Z. Liang, E.S. Choi, R.S. Kadambala, C. Zhang, J.S. Brooks, B. Wang, L. Kramer, *Current Applied Physics*, **2006**, *6*, 119.
[149] A.M. Marconnet, N. Yamamoto, M.A. Panzer, B.L. Wardle, K.E. Goodson, **2011**.
[150] H. Huang, C. Liu, Y. Wu, S. Fan, *Adv. Mater.*, **2005**, *17*, 1652.
[151] J.G. Park, Q. Cheng, J. Lu, J. Bao, S. Li, Y. Tian, Z. Liang, C. Zhang, B. Wang, *Carbon*, **2012**, *50*, 2083.
[152] K. Evanoff, J. Khan, A.A. Balandin, A. Magasinski, W.J. Ready, T.F. Fuller, G. Yushin, *Adv. Mater.*, **2012**, *24*, 533.
[153] M. Oguntoye, S. Oak, L. Pashazanusi, L. Pratt, N.S. Pesika, *Electrochim. Acta*, **2017**, *236*, 408.
[154] a) C. Du, J. Yeh, N. Pan, *Nanotechnology*, **2005**, *16*, 350; b) D.T. Welna, L. Qu, B.E. Taylor, L. Dai, M.F. Durstock, *J. Power Sources*, **2011**, *196*, 1455; c) K. Wang, Y. Wu, H. Wu, Y. Luo, D. Wang, K. Jiang, Q. Li, Y. Li, S. Fan, J. Wang, *J. Power Sources*, **2017**, *351*, 160; d) K. Zhu, Y. Luo, F. Zhao, J. Hou, X. Wang, H. Ma, H. Wu, Y. Zhang, K. Jiang, S. Fan, *ACS Sustainable Chem. Eng.*, **2018**, *6*, 3426.
[155] a) S. Dörfler, M. Hagen, H. Althues, J. Tübke, S. Kaskel, M.J. Hoffmann, *Chem. Commun.*, **2012**, *48*, 4097; b) L. Sun, W. Kong, Y. Jiang, H. Wu, K. Jiang, J. Wang, S. Fan, *Journal of*

Materials Chemistry A, **2015**, *3*, 5305; c) X.-B. Cheng, J.-Q. Huang, Q. Zhang, H.-J. Peng, M.-Q. Zhao, F. Wei, *Nano Energy*, **2014**, *4*, 65; d) Y. Luo, N. Luo, W. Kong, H. Wu, K. Wang, S. Fan, W. Duan, J. Wang, *Small*, **2018**, *14*, 1702853.
[156] Y. Jiang, P. Wang, X. Zang, Y. Yang, A. Kozinda, L. Lin, *Nano Lett.*, **2013**, *13*, 3524.
[157] H. Zhang, G. Cao, Y. Yang, Z. Gu, *J. Electrochem. Soc.*, **2008**, *155*, K19.
[158] W. Wang, R. Epur, P.N. Kumta, *Electrochem. Commun.*, **2011**, *13*, 429.
[159] Y. Wu, Y. Wei, J. Wang, K. Jiang, S. Fan, *Nano Lett.*, **2013**, *13*, 818.
[160] G. Zhang, Y. Song, H. Zhang, J. Xu, H. Duan, J. Liu, *Adv. Funct. Mater.*, **2016**, *26*, 3012.
[161] W. Weng, Q. Sun, Y. Zhang, H. Lin, J. Ren, X. Lu, M. Wang, H. Peng, *Nano Lett.*, **2014**, *14*, 3432.
[162] D.N. Futaba, K. Hata, T. Yamada, T. Hiraoka, Y. Hayamizu, Y. Kakudate, O. Tanaike, H. Hatori, M. Yumura, S. Iijima, *Nat. Mater.*, **2006**, *5*, 987.
[163] T. Lv, Y. Yao, N. Li, T. Chen, *Angew. Chem., Int. Ed.*, **2016**, *55*, 9191.
[164] A.L.M. Reddy, M.M. Shaijumon, S.R. Gowda, P.M. Ajayan, *Nano Lett.*, **2009**, *9*, 1002.
[165] K. Fu, O. Yildiz, H. Bhanushali, Y. Wang, K. Stano, L. Xue, X. Zhang, P.D. Bradford, *Adv. Mater.*, **2013**, *25*, 5109.
[166] a) G. Wu, P. Tan, D. Wang, Z. Li, L. Peng, Y. Hu, C. Wang, W. Zhu, S. Chen, W. Chen, *Sci. Rep.*, **2017**, *7*; b) J. Chen, Y. Liu, A.I. Minett, C. Lynam, J. Wang, G.G. Wallace, *Chem. Mater.*, **2007**, *19*, 3595.
[167] A. Izadi‐Najafabadi, S. Yasuda, K. Kobashi, T. Yamada, D.N. Futaba, H. Hatori, M. Yumura, S. Iijima, K. Hata, *Adv. Mater.*, **2010**, *22*, E235.
[168] A. Izadi-Najafabadi, D.N. Futaba, S. Iijima, K. Hata, *J. Am. Chem. Soc.*, **2010**, *132*, 18017.
[169] J. Di, Z. Yong, Z. Yao, X. Liu, X. Shen, B. Sun, Z. Zhao, H. He, Q. Li, *Small*, **2013**, *9*, 148.
[170] J. Di, Z. Yong, X. Zheng, B. Sun, Q. Li, *Small*, **2013**, *9*, 1367.
[171] H. Murakami, M. Hirakawa, C. Tanaka, H. Yamakawa, *Appl. Phys. Lett.*, **2000**, *76*, 1776.
[172] S. Jo, Y. Tu, Z. Huang, D. Carnahan, D. Wang, Z. Ren, *Appl. Phys. Lett.*, **2003**, *82*, 3520.
[173] Y. Chen, D.T. Shaw, L. Guo, *Appl. Phys. Lett.*, **2000**, *76*, 2469.
[174] J.I. Sohn, S. Lee, Y.-H. Song, S.-Y. Choi, K.-I. Cho, K.-S. Nam, *Appl. Phys. Lett.*, **2001**, *78*, 901.
[175] Y.J. Jung, S. Kar, S. Talapatra, C. Soldano, G. Viswanathan, X. Li, Z. Yao, F.S. Ou, A. Avadhanula, R. Vajtai, *Nano Lett.*, **2006**, *6*, 413.
[176] a) Y. Wang, S. Gupta, J. Garguilo, Z. Liu, L. Qin, R. Nemanich, *Diamond Relat. Mater.*, **2005**, *14*, 714; b) K. Seko, J.-i. Kinoshita, Y. Saito, *Jpn. J. Appl. Phys.*, **2005**, *44*, L743; c) H. Machida, S.-i. Honda, S. Ohkura, K. Oura, H. Inakura, M. Katayama, *Jpn. J. Appl. Phys.*, **2006**, *45*, 1044.
[177] H. Kurachi, "FED with double-walled carbon nanotube emitters", presented at *Proc. 21st IDRC in conjunction with 8th IDW*, **2001**.
[178] T. Yamada, T. Namai, K. Hata, D.N. Futaba, K. Mizuno, J. Fan, M. Yudasaka, M. Yumura, S. Iijima, *Nat. Nanotechnol.*, **2006**, *1*, 131.
[179] S.J. Kang, C. Kocabas, T. Ozel, M. Shim, N. Pimparkar, M.A. Alam, S.V. Rotkin, J.A. Rogers, *Nat. Nanotechnol.*, **2007**, *2*, 230.
[180] J. Li, Q. Zhang, D. Yang, J. Tian, *Carbon*, **2004**, *42*, 2263.
[181] S.J. Kang, C. Kocabas, T. Ozel, M. Shim, N. Pimparkar, M.A. Alam, S.V. Rotkin, J.A. Rogers, *Nat. Nanotechnol.*, **2007**, *2*, 230.
[182] C. Kocabas, S. Dunham, Q. Cao, K. Cimino, X. Ho, H.-S. Kim, D. Dawson, J. Payne, M. Stuenkel, H. Zhang, *Nano Lett.*, **2009**, *9*, 1937.

[183] a) N. Komatsu, W. Gao, P. Chen, C. Guo, A. Babakhani, J. Kono, *Adv. Funct. Mater.*, **2017**, *27*, 1606022; b) M.A. Rahman, J.H. Park, K.T. Truong, D. Suh, G. Scalia, *Photonics Lett. Pol.*, **2017**, *9*, 26.
[184] E. Cubukcu, F. Degirmenci, C. Kocabas, M.A. Zimmler, J.A. Rogers, F. Capasso, *Proc. Natl. Acad. Sci.*, **2009**, *106*, 2495.
[185] K. Liu, Y. Sun, P. Liu, J. Wang, Q. Li, S. Fan, K. Jiang, *Nanotechnology*, **2009**, *20*, 335705.
[186] L. Ren, C.L. Pint, T. Arikawa, K. Takeya, I. Kawayama, M. Tonouchi, R.H. Hauge, J. Kono, *Nano Lett.*, **2012**, *12*, 787.
[187] L. Ren, C.L. Pint, L.G. Booshehri, W.D. Rice, X. Wang, D.J. Hilton, K. Takeya, I. Kawayama, M. Tonouchi, R.H. Hauge, *Nano Lett.*, **2009**, *9*, 2610.
[188] M. Zhang, S. Fang, A.A. Zakhidov, S.B. Lee, A.E. Aliev, C.D. Williams, K.R. Atkinson, R.H. Baughman, *Science*, **2005**, *309*, 1215.
[189] S. Shoji, H. Suzuki, R.P. Zaccaria, Z. Sekkat, S. Kawata, *Phys. Rev. B*, **2008**, *77*, 153407.
[190] W. Fu, L. Liu, K. Jiang, Q. Li, S. Fan, *Carbon*, **2010**, *48*, 1876.
[191] S.J. Kang, C. Kocabas, H.-S. Kim, Q. Cao, M.A. Meitl, D.-Y. Khang, J.A. Rogers, *Nano Lett.*, **2007**, *7*, 3343.
[192] P. Liu, L. Liu, Y. Wei, K. Liu, Z. Chen, K. Jiang, Q. Li, S. Fan, *Adv. Mater.*, **2009**, *21*, 3563.
[193] S.Y. Jeon, S.H. Shin, S.J. Jeong, S.H. Lee, S.H. Jeong, Y.H. Lee, H.C. Choi, K.J. Kim, *Appl. Phys. Lett.*, **2007**, *90*, 121901.
[194] C. Feng, K. Liu, J.S. Wu, L. Liu, J.S. Cheng, Y. Zhang, Y. Sun, Q. Li, S. Fan, K. Jiang, *Adv. Funct. Mater.*, **2010**, *20*, 885.
[195] K. Mizuno, J. Ishii, H. Kishida, Y. Hayamizu, S. Yasuda, D.N. Futaba, M. Yumura, K. Hata, *Proc. Natl. Acad. Sci.*, **2009**, pnas. 0900155106.
[196] a) X. Yu, R. Rajamani, K. Stelson, T. Cui, *Sens. Actuators, A*, **2006**, *132*, 626; b) M. Penza, G. Cassano, P. Aversa, A. Cusano, A. Cutolo, M. Giordano, L. Nicolais, *Nanotechnology*, **2005**, *16*, 2536; c) L. Xiao, Z. Chen, C. Feng, L. Liu, Z.-Q. Bai, Y. Wang, L. Qian, Y. Zhang, Q. Li, K. Jiang, *Nano Lett*, **2008**, *8*, 4539; d) A.E. Aliev, M.D. Lima, S. Fang, R.H. Baughman, *Nano Lett*, **2010**, *10*, 2374; e) A.E. Aliev, J. Oh, M.E. Kozlov, A.A. Kuznetsov, S. Fang, A.F. Fonseca, R. Ovalle, M.D. Lima, M.H. Haque, Y.N. Gartstein, *science*, **2009**, *323*, 1575; f) S.R. Shin, C. Shin, A. Memic, S. Shadmehr, M. Miscuglio, H.Y. Jung, S.M. Jung, H. Bae, A. Khademhosseini, X.S. Tang, *Adv. Funct. Mater.*, **2015**, *25*, 4486; g) Y. Yu, Y. Luo, A. Guo, L. Yan, Y. Wu, K. Jiang, Q. Li, S. Fan, J. Wang, *Nanoscale*, **2017**, *9*, 6716.
[197] J. Foroughi, G.M. Spinks, G.G. Wallace, J. Oh, M.E. Kozlov, S. Fang, T. Mirfakhrai, J.D. Madden, M.K. Shin, S.J. Kim, *Science*, **2011**, 1211220.
[198] Z.-w. Zhou, Q.-h. Yan, C.-h. Liu, S.-s. Fan, *New Carbon Mater.*, **2017**, *32*, 411.
[199] T. Zhang, S. Mubeen, N.V. Myung, M.A. Deshusses, *Nanotechnology*, **2008**, *19*, 332001.
[200] P. He, L. Dai, *Chem. Commun.*, **2004**, *0*, 348.
[201] J.J. Gooding, R. Wibowo, J. Liu, W. Yang, D. Losic, S. Orbons, F.J. Mearns, J.G. Shapter, D.B. Hibbert, *J. Am. Chem. Soc.*, **2003**, *125*, 9006.
[202] S.K. Vashist, D. Zheng, K. Al-Rubeaan, J.H. Luong, F.-S. Sheu, *Biotechnol. Adv.*, **2011**, *29*, 169.
[203] C.B. Jacobs, M.J. Peairs, B.J. Venton, *Anal. Chim. Acta*, **2010**, *662*, 105.
[204] a) M. Gao, L. Dai, G.G. Wallace, *Electroanalysis*, **2003**, *15*, 1089; b) J.J. Gooding, *Electrochim. Acta*, **2005**, *50*, 3049; c) J. Wang, *Electroanalysis*, **2005**, *17*, 7.
[205] K. Sears, L. Dumée, J. Schütz, M. She, C. Huynh, S. Hawkins, M. Duke, S. Gray, *Materials*, **2010**, *3*, 127.
[206] A. López-Lorente, B. Simonet, M. Valcárcel, ACS Publications **2010**.

[207] M. Cinke, J. Li, B. Chen, A. Cassell, L. Delzeit, J. Han, M. Meyyappan, *Chem. Phys. Lett.*, **2002**, *365*, 69.
[208] a) L.F. Dumée, K. Sears, J. Schütz, N. Finn, C. Huynh, S. Hawkins, M. Duke, S. Gray, *J. Membr. Sci.*, **2010**, *351*, 36; b) L. Dumée, K. Sears, J. Schütz, N. Finn, M. Duke, S. Gray, *Proc. ICOM 2018*, **2008**.
[209] G. Viswanathan, D.B. Kane, P.J. Lipowicz, *Adv. Mater.*, **2004**, *16*, 2045.
[210] a) S. Kang, M. Pinault, L.D. Pfefferle, M. Elimelech, *Langmuir*, **2007**, *23*, 8670; b) A.S. Brady‐Estévez, S. Kang, M. Elimelech, *Small*, **2008**, *4*, 481.
[211] a) G. Hummer, J.C. Rasaiah, J.P. Noworyta, *Nature*, **2001**, *414*, 188; b) A.I. Skoulidas, D.M. Ackerman, J.K. Johnson, D.S. Sholl, *Phys. Rev. Lett.*, **2002**, *89*, 185901; c) H. Chen, J.K. Johnson, D.S. Sholl, *The Journal of Physical Chemistry B*, **2006**, *110*, 1971; d) A. Waghe, J.C. Rasaiah, G. Hummer, *The Journal of chemical physics*, **2002**, *117*, 10789; e) A. Noy, H.G. Park, F. Fornasiero, J.K. Holt, C.P. Grigoropoulos, O. Bakajin, *Nano Today*, **2007**, *2*, 22.
[212] a) J.K. Holt, H.G. Park, Y. Wang, M. Stadermann, A.B. Artyukhin, C.P. Grigoropoulos, A. Noy, O. Bakajin, *Science*, **2006**, *312*, 1034; b) B.J. Hinds, N. Chopra, T. Rantell, R. Andrews, V. Gavalas, L.G. Bachas, *Science*, **2004**, *303*, 62; c) J.K. Holt, A. Noy, T. Huser, D. Eaglesham, O. Bakajin, *Published in: Nanoletters, vol. 4, no. 11, September 30, 2004, pp. 2245-2250*, **2004**, *4*.
[213] M. Yu, H.H. Funke, J.L. Falconer, R.D. Noble, *Nano Lett.*, **2008**, *9*, 225.
[214] H. Liu, J. Zhai, L. Jiang, *Soft Matter*, **2006**, *2*, 811.
[215] a) H.G. Schild, *Prog. Polym. Sci.*, **1992**, *17*, 163; b) Z. Hu, Y. Chen, C. Wang, Y. Zheng, Y. Li, *Nature*, **1998**, *393*, 149.
[216] J. Bico, C. Marzolin, D. Quéré, *EPL (Europhysics Letters)*, **1999**, *47*, 220.
[217] L. Feng, S. Li, Y. Li, H. Li, L. Zhang, J. Zhai, Y. Song, B. Liu, L. Jiang, D. Zhu, *Adv. Mater.*, **2002**, *14*, 1857.
[218] C.K. Chua, K.F. Leong, *3D Printing and Additive Manufacturing: Principles and Applications (with Companion Media Pack) of Rapid Prototyping Fourth Edition*, World Scientific Publishing Company**2014**.
[219] a) M. Shofner, K. Lozano, F. Rodríguez‐Macías, E. Barrera, *J. Appl. Polym. Sci.*, **2003**, *89*, 3081; b) N. Aliheidari, C. Hohimer, A. Ameli, "3D-Printed Conductive Nanocomposites for Liquid Sensing Applications", presented at *ASME 2017 Conference on Smart Materials, Adaptive Structures and Intelligent Systems*, **2017**.
[220] L.L. Lebel, B. Aissa, M.A.E. Khakani, D. Therriault, *Adv. Mater.*, **2010**, *22*, 592.
[221] G. Tsiakatouras, E. Tsellou, C. Stergiou, *World Transactions on Engineering and Technology Education*, **2014**, *12*, 392.
[222] G. Postiglione, G. Natale, G. Griffini, M. Levi, S. Turri, *Composites, Part A*, **2015**, *76*, 110.
[223] J.P. Lewicki, J.N. Rodriguez, C. Zhu, M.A. Worsley, A.S. Wu, Y. Kanarska, J.D. Horn, E.B. Duoss, J.M. Ortega, W. Elmer, *Sci. Rep.*, **2017**, *7*, 43401.
[224] P. Calvert, R. Crockett, *Chem. Mater.*, **1997**, *9*, 650.
[225] E.D. Yildirim, X. Yin, K. Nair, W. Sun, *Journal of Biomedical Materials Research Part B: Applied Biomaterials: An Official Journal of The Society for Biomaterials, The Japanese Society for Biomaterials, and The Australian Society for Biomaterials and the Korean Society for Biomaterials*, **2008**, *87*, 406.
[226] J. He, F. Xu, R. Dong, B. Guo, D. Li, *Biofabrication*, **2017**, *9*, 015007.
[227] C. Mahajan, D. Cormier, "3D Printing of Carbon Fiber Composites With Preferentially Aligned Fibers", presented at *IIE Annual Conference. Proceedings*, **2015**.
[228] O. Ivanova, C. Williams, T. Campbell, *Rapid Prototyping Journal*, **2013**, *19*, 353.
[229] J. Xie, N. Zhang, M. Guers, V.K. Varadan, *Smart Mater. Struct.*, **2002**, *11*, 575.

[230] K.S. Wagner, Investigate methods to increase the usefulness of stereolithography 3D printed objects by adding carbon nanotubes to photo-curable resins, University of Minnesota Duluth, http://hdl.handle.net/10792/1209, **2014**
[231] a) J. Hector Sandoval, R.B. Wicker, *Rapid Prototyping Journal*, **2006**, *12*, 292; b) J. Sandoval, K. Soto, L. Murr, R. Wicker, *J. Mater. Sci.*, **2007**, *42*, 156.
[232] Y. Yang, Z. Chen, X. Song, Z. Zhang, J. Zhang, K.K. Shung, Q. Zhou, Y. Chen, *Adv. Mater.*, **2017**, *29*, 1605750.
[233] a) S. Yuan, J. Bai, C.K. Chua, J. Wei, K. Zhou, *Polymers*, **2016**, *8*, 370; b) J. Bai, S. Yuan, F. Shen, B. Zhang, C.K. Chua, K. Zhou, J. Wei, *Virtual and Physical Prototyping*, **2017**, *12*, 235.
[234] K. Chen, W. Gao, S. Emaminejad, D. Kiriya, H. Ota, H.Y.Y. Nyein, K. Takei, A. Javey, *Adv. Mater.*, **2016**, *28*, 4397.
[235] a) C.S. Jones, X. Lu, M. Renn, M. Stroder, W.-S. Shih, *Microelectron. Eng.*, **2010**, *87*, 434; b) G.L. Goh, S. Agarwala, Y.J. Tan, W.Y. Yeong, *Sens. Actuators, B*, **2018**, *260*, 227.
[236] a) S. Azoubel, S. Shemesh, S. Magdassi, *Nanotechnology*, **2012**, *23*, 344003; b) A. Denneulin, J. Bras, F. Carcone, C. Neuman, A. Blayo, *Carbon*, **2011**, *49*, 2603.
[237] Q. Cao, H.-s. Kim, N. Pimparkar, J.P. Kulkarni, C. Wang, M. Shim, K. Roy, M.A. Alam, J.A. Rogers, *Nature*, **2008**, *454*, 495.
[238] a) G.L. Goh, S. Agarwala, Y.J. Tan, W.Y. Yeong, *Sens. Actuators, B*, **2017**; b) H.M. L., C. Alex, T.B. C.-K., T.J. B.-H., B. Zhenan, *Adv. Mater.*, **2013**, *25*, 5997.
[239] V.K. Sangwan, R.P. Ortiz, J.M. Alaboson, J.D. Emery, M.J. Bedzyk, L.J. Lauhon, T.J. Marks, M.C. Hersam, *Acs Nano*, **2012**, *6*, 7480.
[240] M.F.L. De Volder, S.H. Tawfick, R.H. Baughman, A.J. Hart, *Science*, **2013**, *339*, 535.
[241] M. Zarek, M. Layani, I. Cooperstein, E. Sachyani, D. Cohn, S. Magdassi, *Adv. Mater.*, **2016**, *28*, 4449.
[242] a) W. Yu, H. Zhou, B.Q. Li, S. Ding, *ACS Appl. Mater. Interfaces*, **2017**, *9*, 4597; b) J. Vaillancourt, H. Zhang, P. Vasinajindakaw, H. Xia, X. Lu, X. Han, D.C. Janzen, W.-S. Shih, C.S. Jones, M. Stroder, *Appl. Phys. Lett.*, **2008**, *93*, 444; c) N. Saengchairat, T. Tran, C.-K. Chua, *Virtual and Physical Prototyping*, **2017**, *12*, 31.
[243] B. Ando, S. Baglio, *IEEE Sens. J.*, **2013**, *13*, 4874.
[244] F. Villani, I. Grimaldi, T. Polichetti, E. Massera, A.D.G. Del Mauro, G. Di Francia, "Inkjet Printed Chemical Sensors", presented at *Sensors and Microsystems*, Italy, **2010**.
[245] H. Tan, T. Tran, C. Chua, *Virtual and Physical Prototyping*, **2016**, *11*, 271.
[246] J. Chang, T. Ge, E. Sanchez-Sinencio, "Challenges of printed electronics on flexible substrates", presented at *Circuits and Systems (MWSCAS), 2012 IEEE 55th International Midwest Symposium on*, **2012**.
[247] M. Ha, J.-W.T. Seo, P.L. Prabhumirashi, W. Zhang, M.L. Geier, M.J. Renn, C.H. Kim, M.C. Hersam, C.D. Frisbie, *Nano Lett.*, **2013**, *13*, 954.
[248] M. Gao, L. Li, Y. Song, *Journal of Materials Chemistry C*, **2017**, *5*, 2971.
[249] L. Cai, C. Wang, in *Flexible and Stretchable Medical Devices*, (Eds: K. Takei), Wiley, **2018**, 7.
[250] A. Brunet, U. Gengenbach, T. Müller, S. Scholz, M. Dickerhof, in *Micro-Manufacturing Technologies and Their Applications*, (Eds: I. Fassi, D. Shipley), Springer, **2017**, 175.
[251] T. Fischer, N. Wetzold, H. Elsner, L. Kroll, A.C. Hübler, *Nanomater. Nanotechnol.*, **2011**, *1*, 18.
[252] H. Shen, T. Liu, D. Qin, X. Bo, L. Wang, F. Wang, Q. Yuan, T. Wagberg, G. Hu, M. Zhou, in *Industrial Applications of Carbon Nanotubes*, (Eds: H. Peng, Q. Li, T. Chen), Elsevier, **2017**, 179.
[253] a) P. Chen, H. Chen, J. Qiu, C. Zhou, *Nano Res.*, **2010**, *3*, 594; b) B. Chen, Y. Jiang, X. Tang, Y. Pan, S. Hu, *ACS Appl. Mater. Interfaces*, **2017**, *9*, 28433.

[254] a) X. Wang, J. Li, H. Song, H. Huang, J. Gou, *ACS Appl. Mater. Interfaces*, **2018**, *10*, 7371; b) J.F. Christ, N. Aliheidari, A. Ameli, P. Pötschke, *Mater. Des.*, **2017**, *131*, 394.
[255] J. DeGraff, R. Liang, M.Q. Le, J.-F. Capsal, F. Ganet, P.-J. Cottinet, *Mater. Des.*, **2017**, *133*, 47.
[256] P. Lorwongtragool, E. Sowade, N. Watthanawisuth, R.R. Baumann, T. Kerdcharoen, *Sensors*, **2014**, *14*, 19700.
[257] a) C. Cao, J.B. Andrews, A.D. Franklin, *Adv. Electron. Mater.*, **2017**, *3*, 1700057; b) J. Liang, L. Li, D. Chen, T. Hajagos, Z. Ren, S.-Y. Chou, W. Hu, Q. Pei, *Nat. Commun.*, **2015**, *6*, 7647.
[258] S.R. Shin, R. Farzad, A. Tamayol, V. Manoharan, P. Mostafalu, Y.S. Zhang, M. Akbari, S.M. Jung, D. Kim, M. Comotto, *Adv. Mater.*, **2016**, *28*, 3280.
[259] Z. Liu, L. Jiao, Y. Yao, X. Xian, J. Zhang, *Adv. Mater.*, **2010**, *22*, 2285.

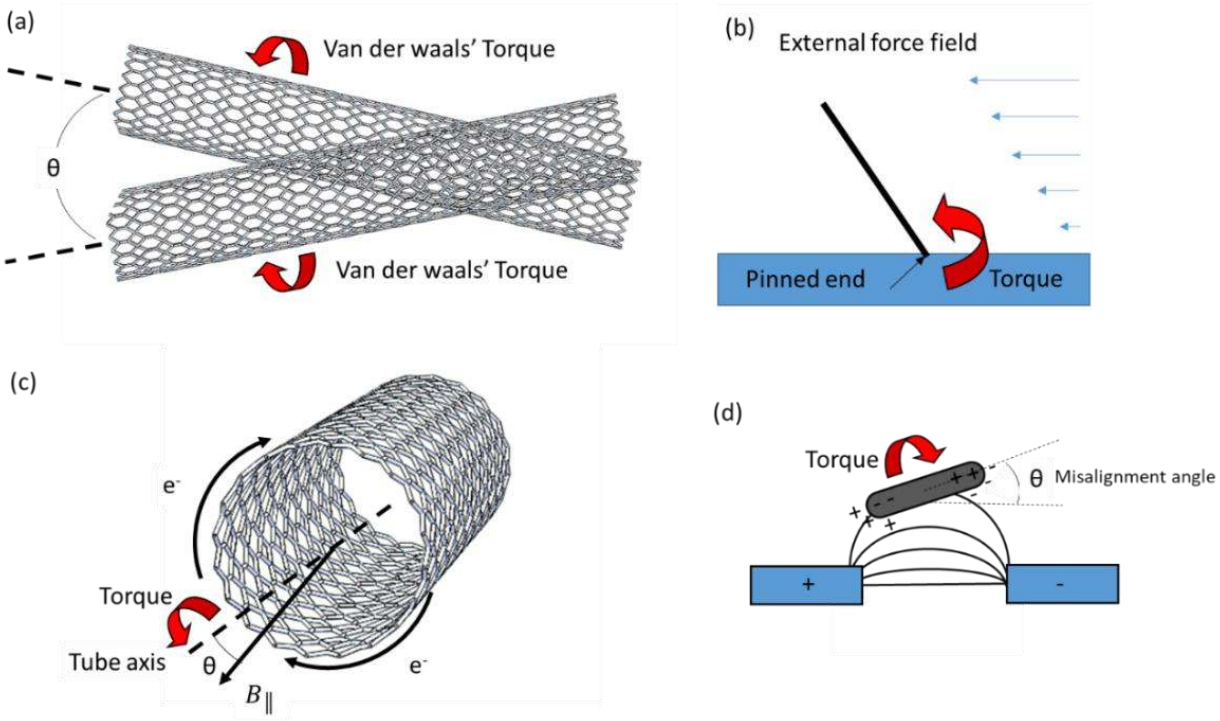

Figure 1. Schematic showing different types of CNT alignment torque (a) van der waals' torque, (b) torque induced by external force on a pinned end of CNT, (c) magnetic-induced torque, and (d) dielectropherosis-induced torque.

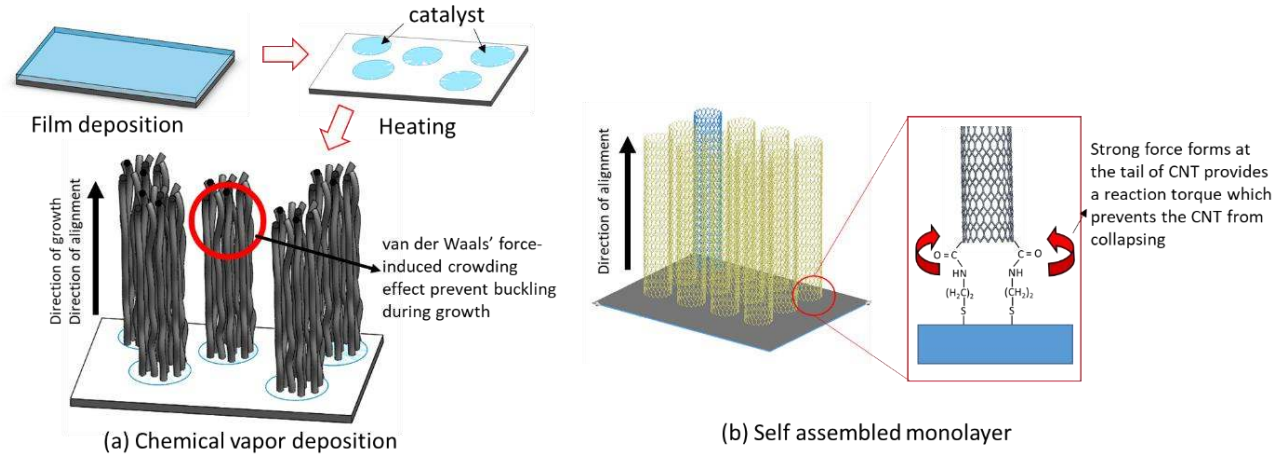

Figure 2. Vertically aligned CNT fabricated by (a) chemical vapor deposition,[31] and (b) self-assembled monolayer as a result of strong van der waal's interaction between the nanotubes and the substrate respectively.[44]

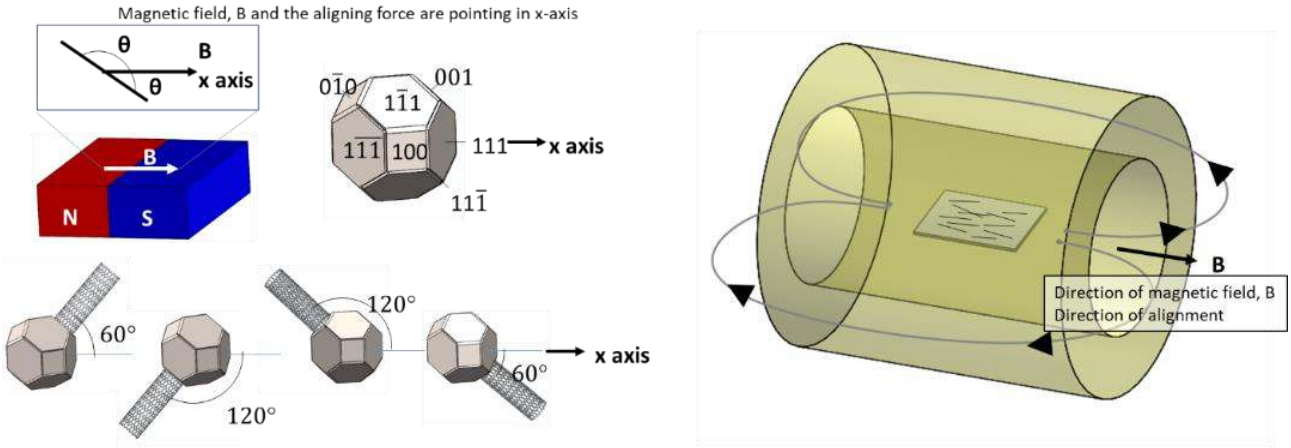

Figure 3. Magnetic field-induced alignment for (a) growth of aligned CNT[47] and (b) solution-processed/composite CNT.[11, 48]

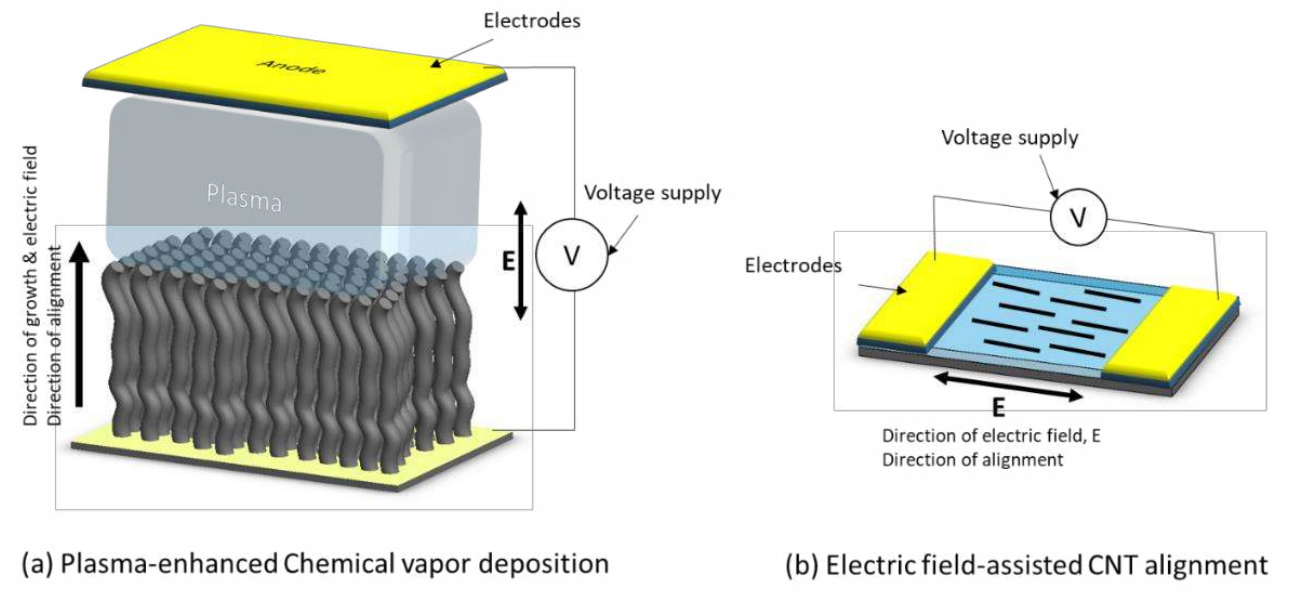

Figure 4. Electric field-induced CNT alignment for (a) growth of VACNT via Plasma-enhanced chemical vapor deposition[58] and (b) solution-processed CNT by applying voltage across 2 terminals.[23, 63]

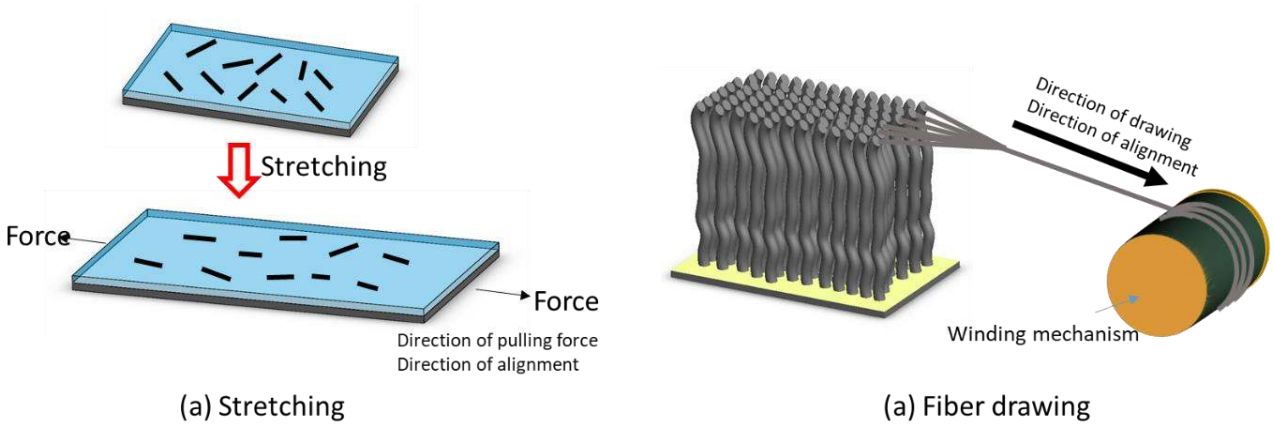

Figure 5. Aligning CNT by (a) stretching method[69] and (b) fiber drawing method.[75]

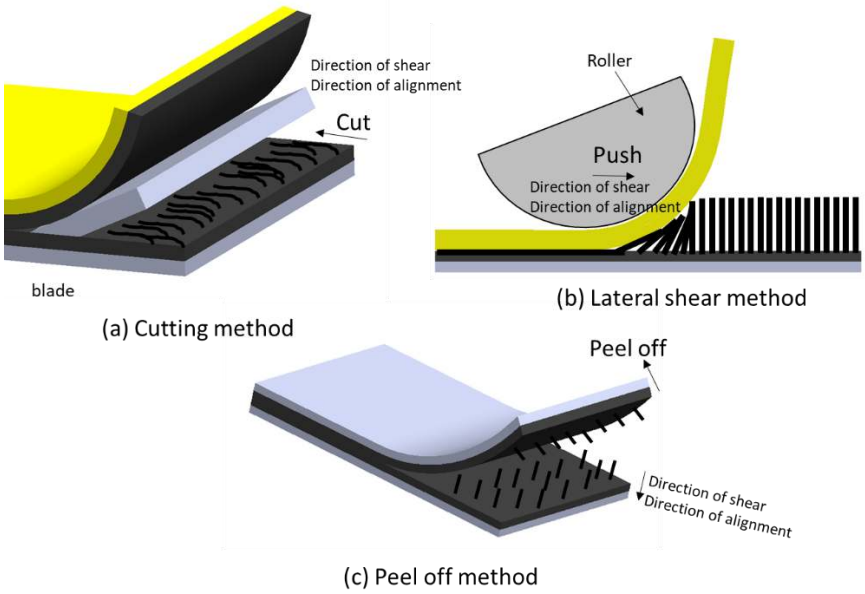

Figure 6. Shear-induced CNT alignment via (a) cutting method,[80] (b) lateral shear method,[83] and (c) peel-off method.[86]

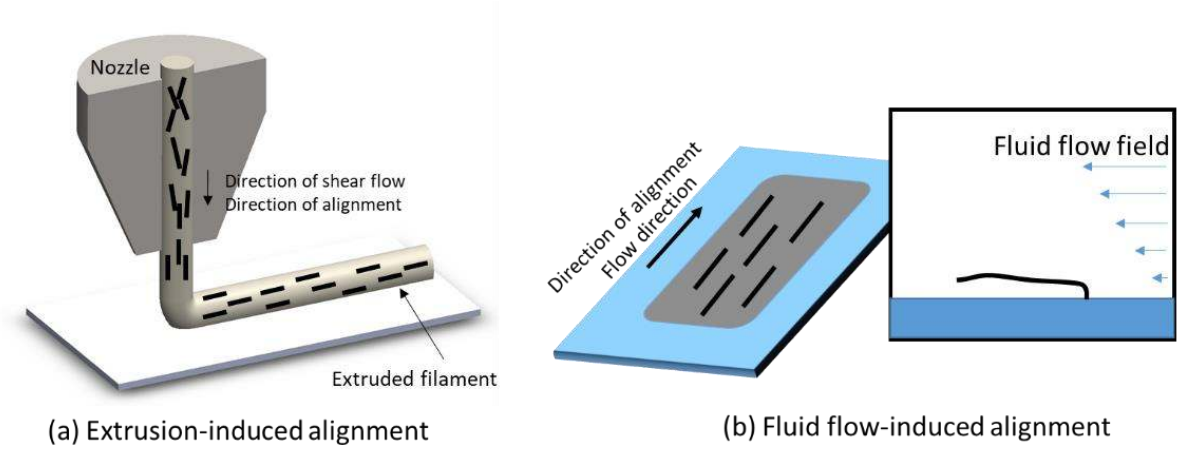

Figure 7. Shear-induced alignment via (a) extrusion process[93] and (b) fluid flow.[104]

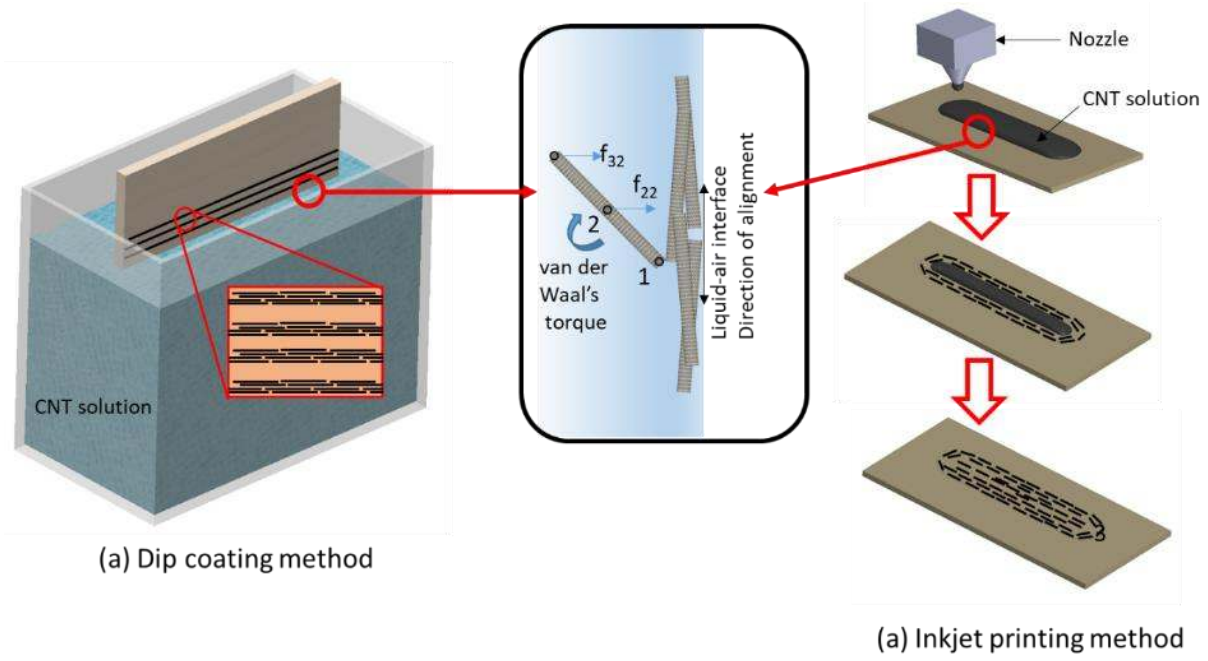

Figure 8. Self-assembly method by (a) dip coating method[117] and (b) inkjet printing method.[118]

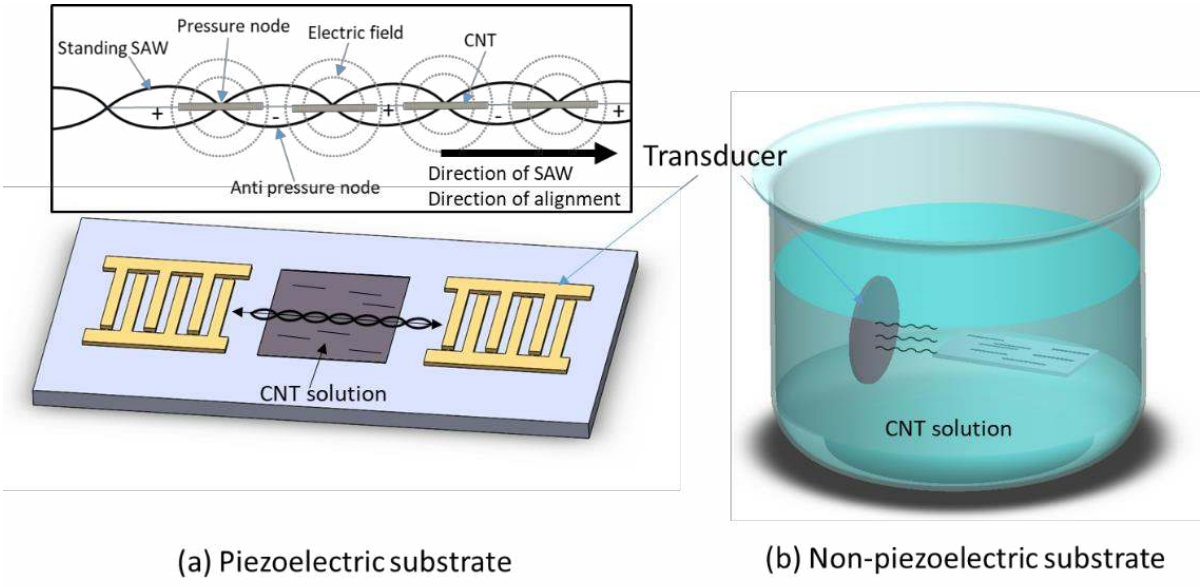

Figure 9. Surface acoustic wave-induced alignment using (a) piezoelectric substrate[131] and (b)non-piezoelectric substrate.[21]

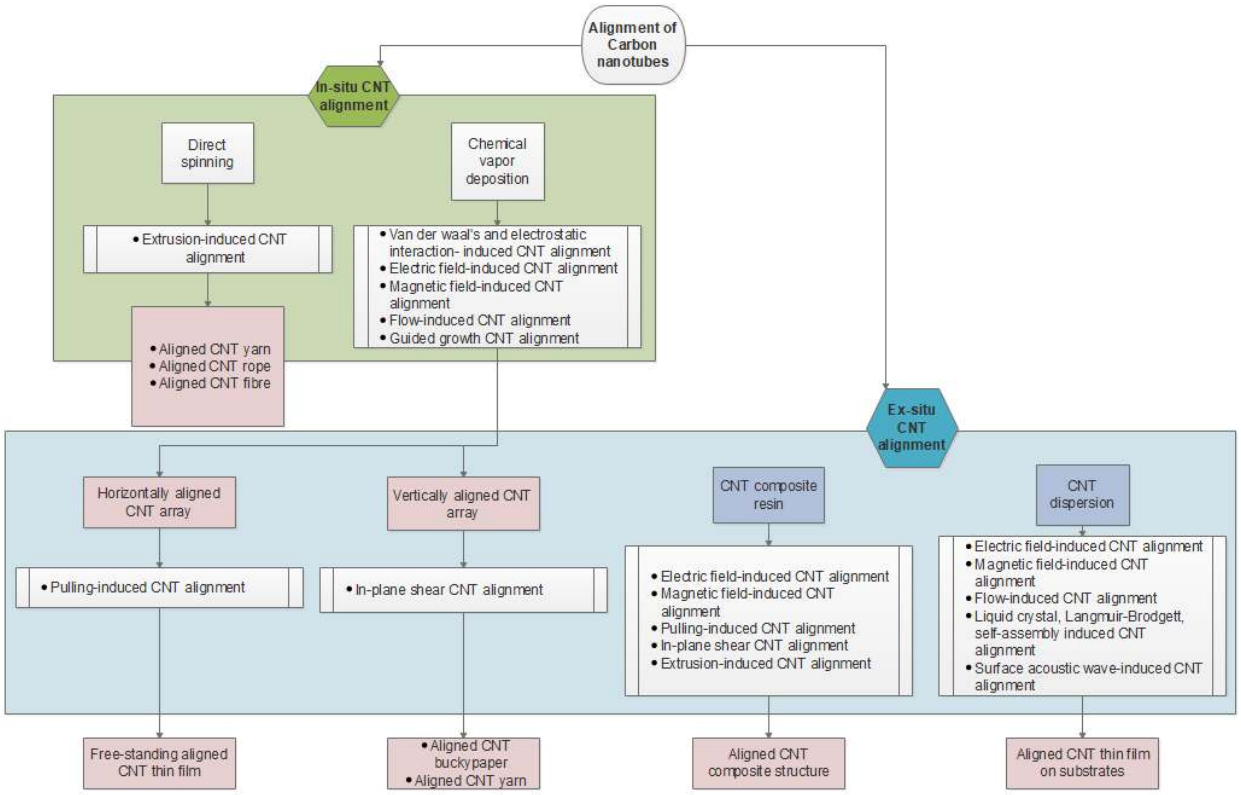

Figure 10. Flowchart showing in-situ and ex-situ CNT alignment techniques and their respective final CNT architectures.

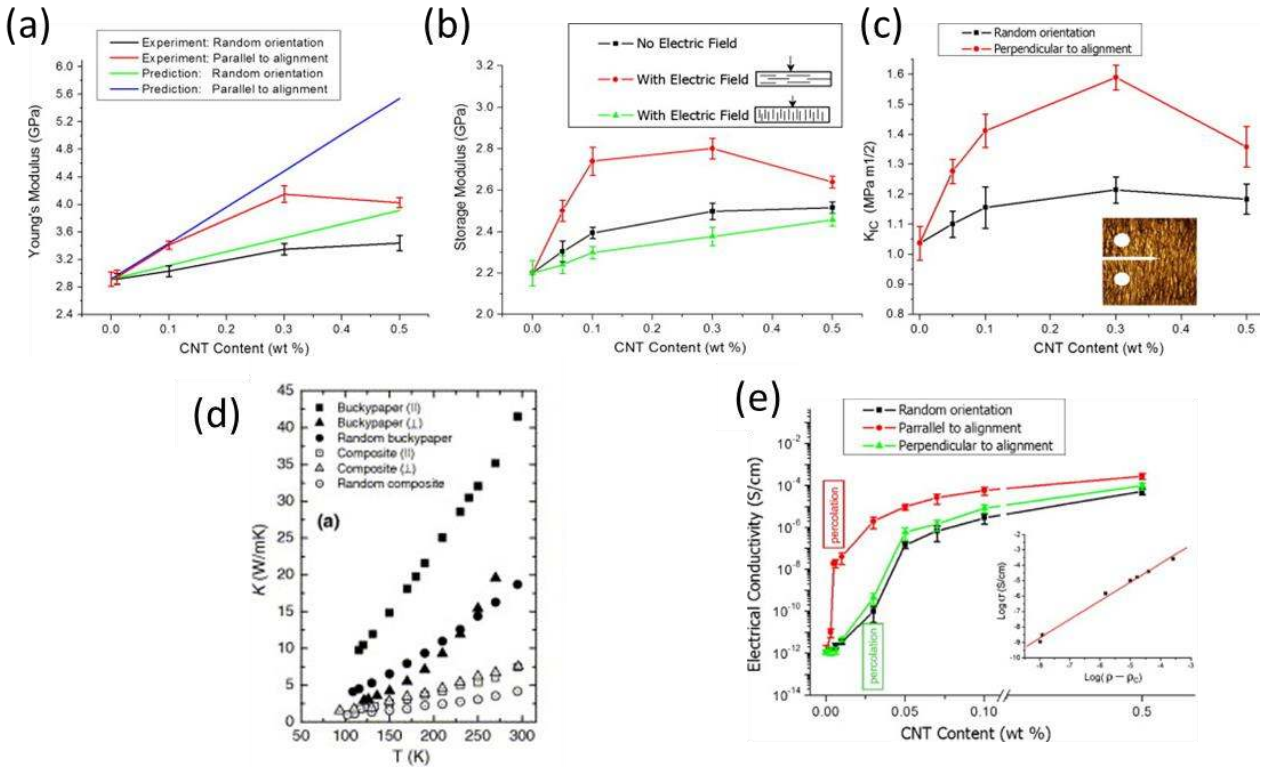

Figure 11. Graphs showing the difference in properties of CNT-composite structure with aligned CNT and random orientation. The 5 properties are (a) Young's Modulus, (b) storage modulus, (c) fracture toughness, (d) thermal conductivity, and (e) electrical conductivity. *Reproduced with permission,* [67], [148] *Copyright 2018, Elsevier.*

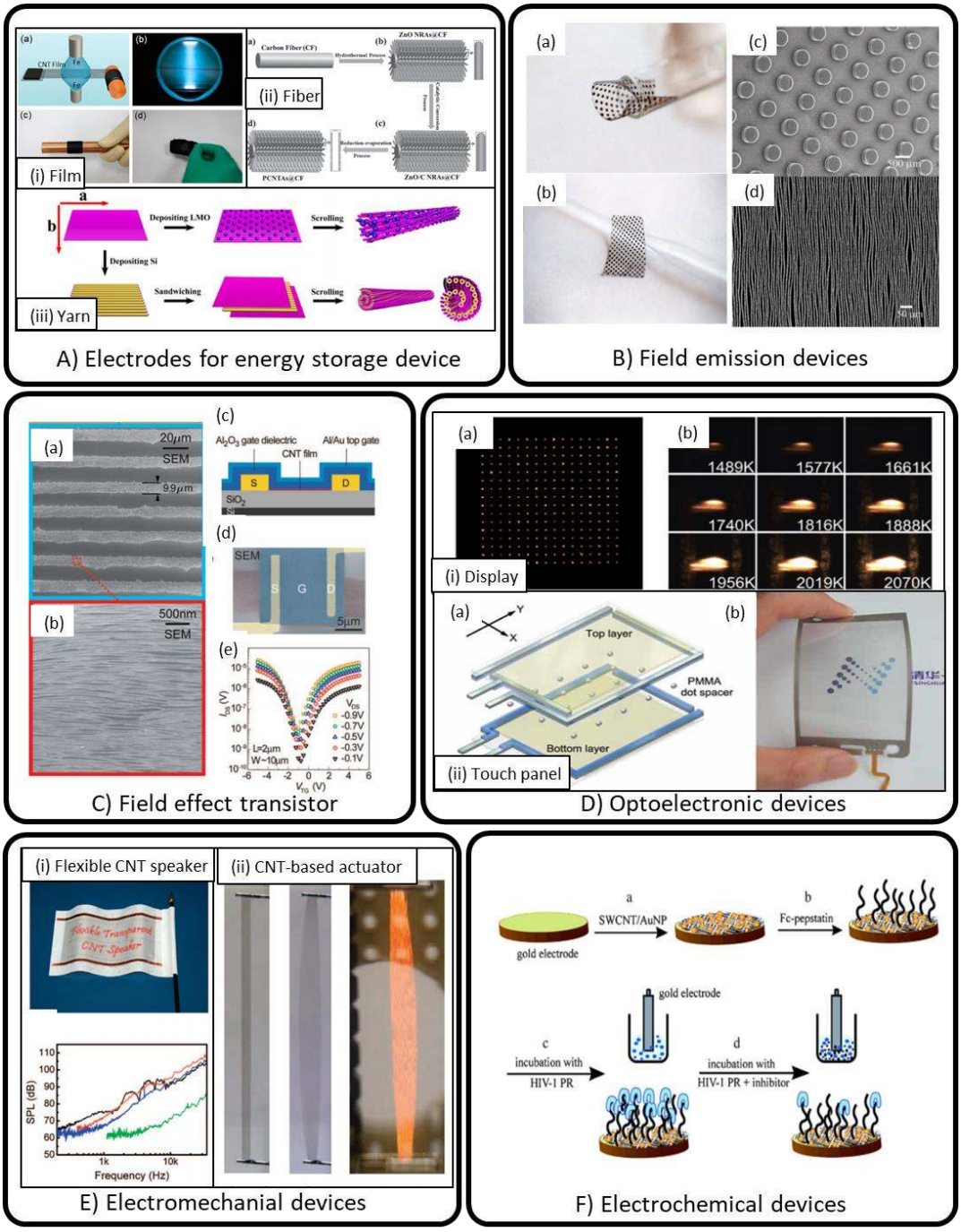

Figure 12. Different electrical and electronic devices, (A) electrodes for energy storage devices, *Reproduced with permission,* [159], [161] *Copyright 2018, American Chemical Society and* [160] *Copyright 2018, John Wiley and Sons.*, (B) field emission devices, *Reproduced with permission,* [175] *Copyright 2018, American Chemical Society*, (C) field effect transistor, *Reproduced with permission,* [124] *Copyright 2018, American Chemical Society*, (D) Optoelectronics devices, (i) a CNT based

display and (ii) a touch panel, *Reproduced with permission, [192], [194] Copyright 2018, John Wiley and Sons*, (E) Electromechanical devices, (i) a flexible CNT speaker and (ii) CNT-based actuator, *Reproduced with permission, [196c] Copyright 2018, John Wiley and Sons, [196e] Copyright 2018, The American Association for the Advancement of Science,* (F) electrochemical devices, *Reproduced with permission, [202] Copyright 2018, Elsevier.*

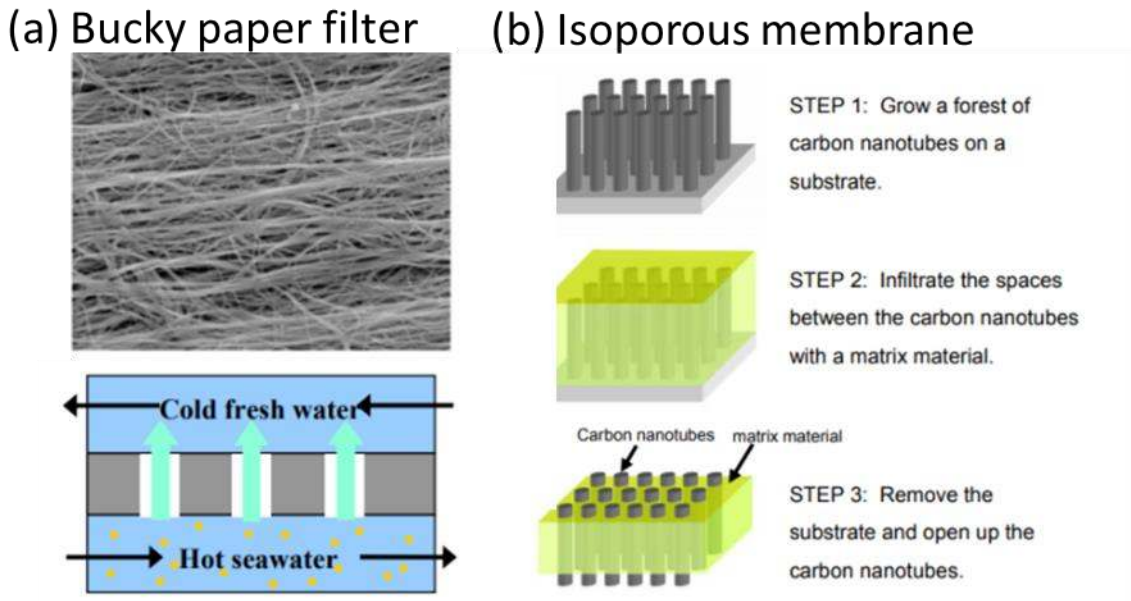

Figure 13. Different types of CNT-based filter, (a) bucky paper filter and (b) isoporous membrane. *Images retrieved from original article by Sears et al. [205].*

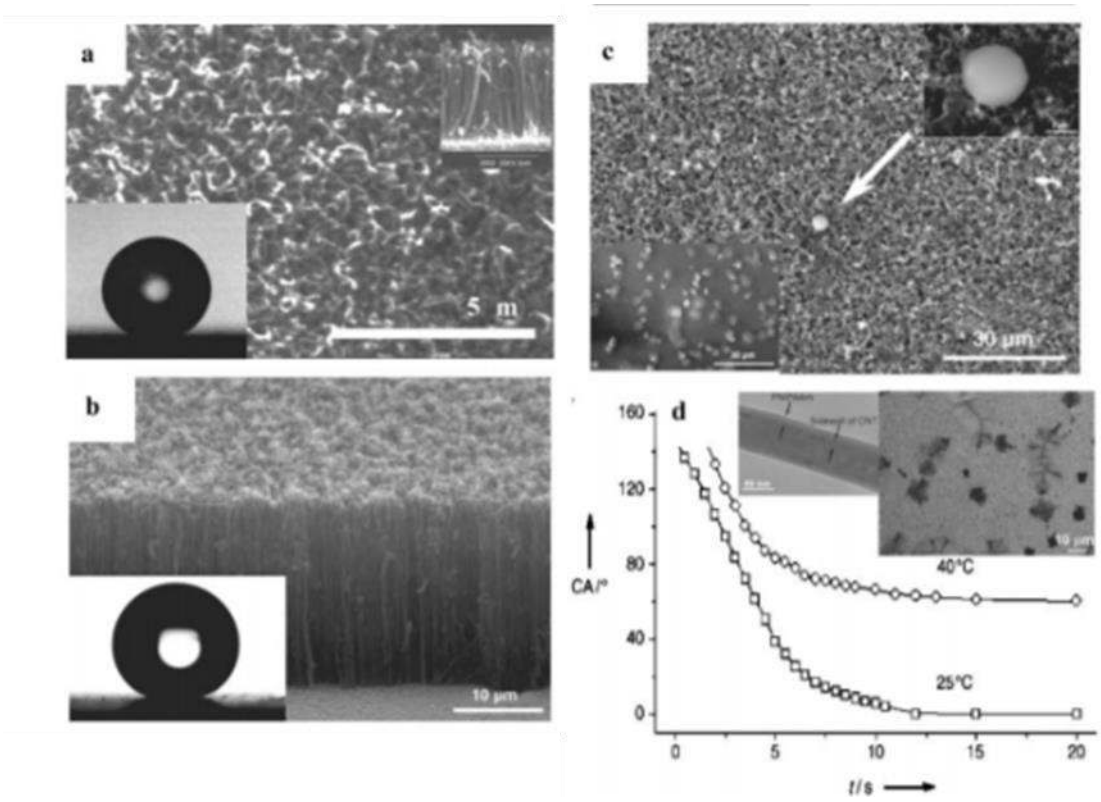

Figure 14. Images showing different types of CNT-based superhydrophobic surfaces. *Reproduced from [214] with permission from the Royal Society of Chemistry.*

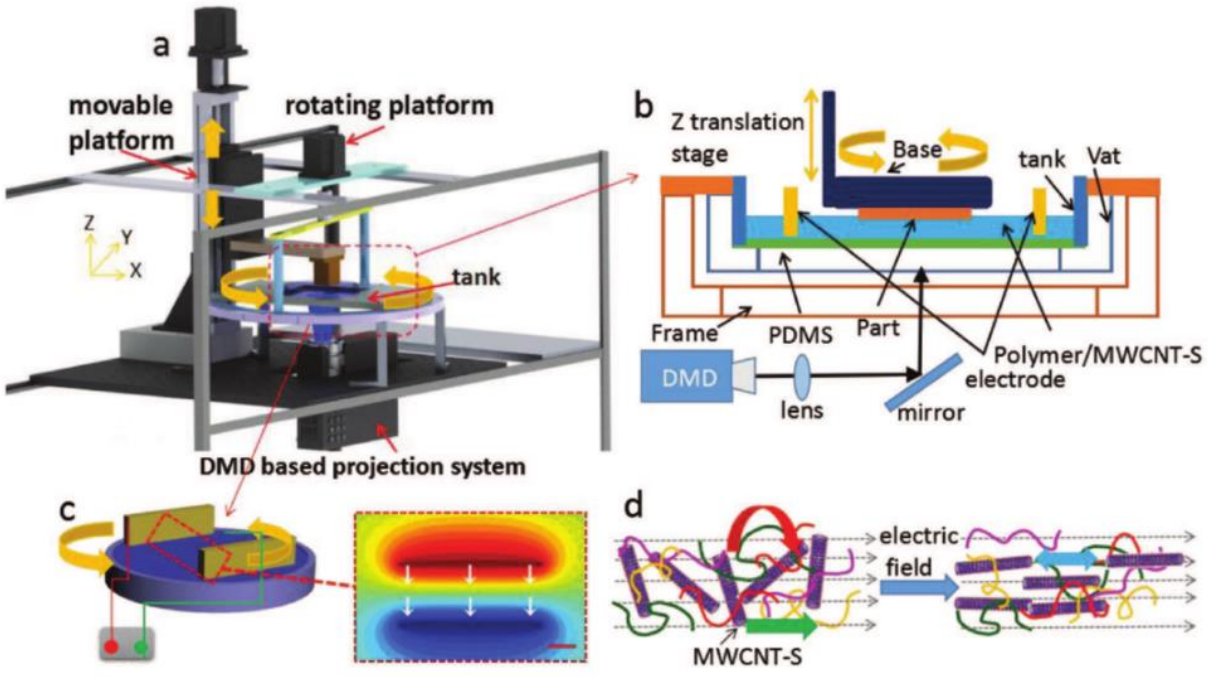

Figure 15. Schematic showing the electrical-assisted stereolithography 3D printing system. *Reproduced with permission, [232] Copyright 2018, John Wiley and Sons.*

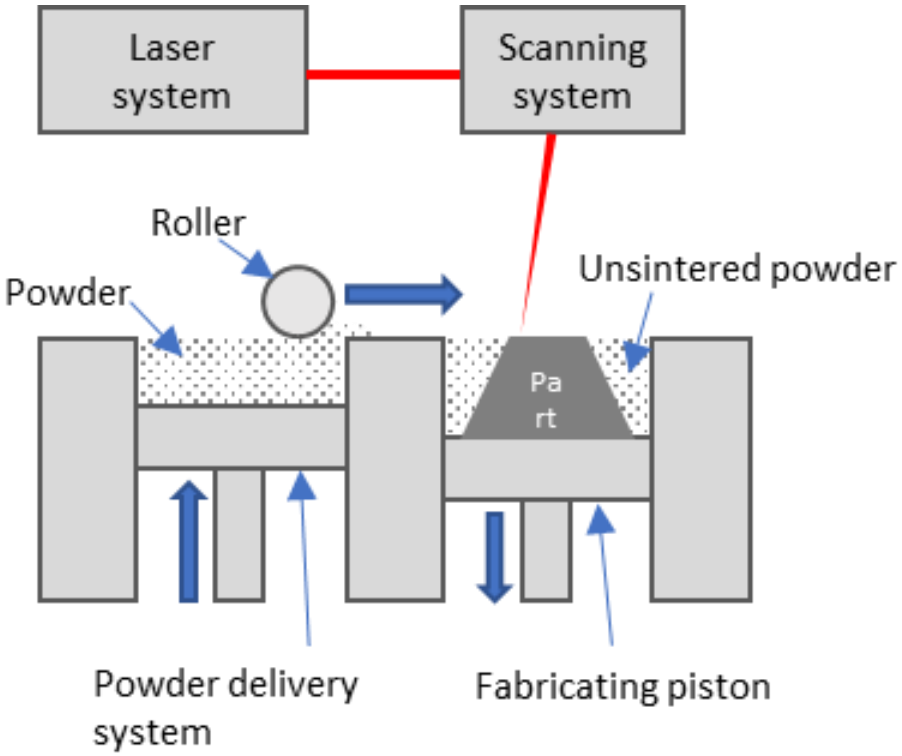

Figure 16. Schematic showing the printing mechanism of powder bed fusion 3D printing technique.

Figure captions

Figure 1. Schematic showing different types of CNT alignment torque (a) van der waals' torque, (b) torque induced by external force on a pinned end of CNT, (c) magnetic-induced torque, and (d) dielectropherosis-induced torque.

Figure 2. Vertically aligned CNT fabricated by (a) chemical vapor deposition,[31] and (b) self-assembled monolayer as a result of strong van der waal's interaction between the nanotubes and the substrate respectively.[44]

Figure 3. Magnetic field-induced alignment for (a) growth of aligned CNT[47] and (b) solution-processed/composite CNT.[11, 48]

Figure 4. Electric field-induced CNT alignment for (a) growth of VACNT via Plasma-enhanced chemical vapor deposition[58] and (b) solution-processed CNT by applying voltage across 2 terminals.[23, 63]

Figure 5. Aligning CNT by (a) stretching method[69] and (b) fiber drawing method.[75]

Figure 6. Shear-induced CNT alignment via (a) cutting method,[80] (b) lateral shear method,[83] and (c) peel-off method.[86]

Figure 7. Shear-induced alignment via (a) extrusion process[93] and (b) fluid flow.[104]

Figure 8. Self-assembly method by (a) dip coating method[117] and (b) inkjet printing method.[118]

Figure 9. Surface acoustic wave-induced alignment using (a) piezoelectric substrate[131] and (b)non-piezoelectric substrate.[21]

Figure 10. Flowchart showing in-situ and ex-situ CNT alignment techniques and their respective final CNT architectures.

Figure 11. Graphs showing the difference in properties of CNT-composite structure with aligned CNT and random orientation. The 5 properties are (a) Young's Modulus, (b) storage modulus, (c) fracture toughness, (d) thermal conductivity, and (e) electrical conductivity. *Reproduced with permission, [67], [148] Copyright 2018, Elsevier.*

Figure 12. Different electrical and electronic devices, (A) electrodes for energy storage devices, *Reproduced with permission, [159], [161] Copyright 2018, American Chemical Society and [160] Copyright 2018, John Wiley and Sons.*, (B) field emission devices, *Reproduced with permission, [175] Copyright 2018, American Chemical Society*, (C) field effect transistor, *Reproduced with permission, [124] Copyright 2018, American Chemical Society*, (D) Optoelectronics devices, (i) a CNT based display and (ii) a touch panel, *Reproduced with permission, [192], [194] Copyright 2018, John Wiley*

and Sons, (E) Electromechanical devices, (i) a flexible CNT speaker and (ii) CNT-based actuator, *Reproduced with permission, [196c] Copyright 2018, John Wiley and Sons, [196e] Copyright 2018, The American Association for the Advancement of Science,* (F) electrochemical devices, *Reproduced with permission, [202] Copyright 2018, Elsevier.*

Figure 13. Different types of CNT-based filter, (a) bucky paper filter and (b) isoporous membrane. *Images retrieved from original article by Sears et al. [205].*

Figure 14. Images showing different types of CNT-based superhydrophobic surfaces. *Reproduced from [214] with permission from the Royal Society of Chemistry.*

Figure 15. Schematic showing the electrical-assisted stereolithography 3D printing system. *Reproduced with permission, [232] Copyright 2018, John Wiley and Sons.*

Figure 16. Schematic showing the printing mechanism of powder bed fusion 3D printing technique.